Atomic Layer Deposition: An Overview

Steven M. George*

Department of Chemistry and Biochemistry and Department of Chemical and Biological Engineering, University of Colorado, Boulder, Colorado 80309

Received February 12, 2009

Contents

Steven M. George is Professor in the Department of Chemistry and Biochemistry and Department of Chemical and Biological Engineering at the University of Colorado at Boulder. Dr. George received his B.S. in Chemistry from Yale University (1977) and his Ph.D. in Chemistry from the University of California at Berkeley (1983). Prior to his appointments at the University of Colorado at Boulder, Dr. George was a Bantrell Postdoctoral Fellow at Caltech (1983−4) and an Assistant Professor in the Department of Chemistry at Stanford University (1984−1991). Dr. George is a Fellow of the American Vacuum Society (2000) and a Fellow of the American Physical Society (1997). He has also received the American Chemical Society Colorado Section Award (2004), R&D 100 Award for Particle-ALD (2004), NSF Presidential Young Investigator Award (1988−1993), and an Alfred P. Sloan Foundation Fellowship (1988). Dr. George's research interests are in the areas of surface chemistry, thin film growth, and nanostructure engineering. He is currently directing a research effort focusing on atomic layer deposition (ALD) and molecular layer deposition (MLD). This research is examining new surface chemistries for ALD and MLD growth, measuring thin film growth rates, and characterizing the properties of thin films. Dr. George served as Chair of the first American Vacuum Society (AVS) Topical Conference on Atomic Layer Deposition (ALD2001) held in Monterey, California. He also teaches a one-day short course on ALD for the AVS. Dr. George is a cofounder of ALD NanoSolutions, Inc., a startup company that is working to commercialize ALD technology.

1. Introduction

Atomic layer deposition (ALD) has emerged as an important technique for depositing thin films for a variety of applications. Semiconductor processing has been one of the main motivations for the recent development of ALD. The *International Technology Roadmap for Semiconductors* (ITRS) has included ALD for high dielectric constant gate oxides in the MOSFET structure and for copper diffusion barriers in backend interconnects.[1] In addition, ALD has met challenging requirements in other areas including the deposition of high quality dielectrics to fabricate trench capacitors for DRAM.[2]

Miniaturization in the semiconductor industry has led to the requirement for atomic level control of thin film deposition. Miniaturization has produced very high aspect structures that need to be coated conformally. No other thin film technique can approach the conformality achieved by ALD on high aspect structures. The necessity for continuous and pinhole-free films in semiconductor devices has driven the advancement of ALD. Other applications with similar demanding requirements outside of the semiconductor industry are low electron leakage dielectrics for magnetic read/write heads[3] and diffusion barrier coatings with low gas permeability.[4]

* E-mail address: Steven.George@Colorado.Edu.

10.1021/cr900056b
Published on Web 11/30/2009

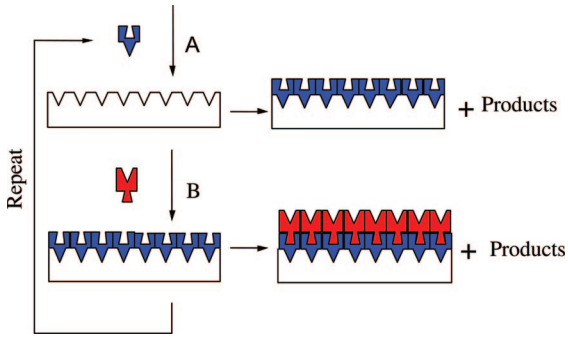

Figure 1. Schematic representation of ALD using self-limiting surface chemistry and an AB binary reaction sequence. (Reprinted with permission from ref 5. Copyright 1996 American Chemical Society.)

ALD is able to meet the needs for atomic layer control and conformal deposition using sequential, self-limiting surface reactions. A schematic showing the sequential, self-limiting surface reactions during ALD is displayed in Figure 1.[5] Most ALD processes are based on binary reaction sequences where two surface reactions occur and deposit a binary compound film. Because there are only a finite number of surface sites, the reactions can only deposit a finite number of surface species. If each of the two surface reactions is self-limiting, then the two reactions may proceed in a sequential fashion to deposit a thin film with atomic level control.

The advantages of ALD are precise thickness control at the Ångstrom or monolayer level. The self-limiting aspect of ALD leads to excellent step coverage and conformal deposition on high aspect ratio structures. Some surface areas will react before other surface areas because of different precursor gas fluxes. However, the precursors will adsorb and subsequently desorb from the surface areas where the reaction has reached completion. The precursors will then proceed to react with other unreacted surface areas and produce a very conformal deposition.

The self-limiting nature of the surface reactions also produces a nonstatistical deposition because the randomness of the precursor flux is removed as an important factor. As a result, ALD films remain extremely smooth and conformal to the original substrate because the reactions are driven to completion during every reaction cycle.[6] Because no surface sites are left behind during film growth, the films tend to be very continuous and pinhole-free. This factor is extremely important for the deposition of excellent dielectric films.[7]

ALD processing is also extendible to very large substrates and to parallel processing of multiple substrates. The ALD precursors are gas phase molecules, and they fill all space independent of substrate geometry and do not require line-of-sight to the substrate. ALD is only limited by the size of the reaction chamber. The ALD process is also dominated by surface reactions. Because the surface reactions are performed sequentially, the two gas phase reactants are not in contact in the gas phase. This separation of the two reactions limits possible gas phase reactions that can form particles that could deposit on the surface to produce granular films.

The use of the term "ALD" dates back approximately to 2000. Prior to 2000, the term atomic layer epitaxy (ALE) was in common use.[8−13] Other terms have been used to describe ALD, including binary reaction sequence chemistry[14] and molecular layer epitaxy.[15] The transition from ALE to ALD occurred as a result of the fact that most films grown using sequential, self-limiting surface reactions were not epitaxial to their underlying substrates. Moreover, amorphous films were most preferred for dielectric and diffusion barrier applications. Consequently, the use of ALD grew in preference and now dominates with the practitioners in the field.

The history of ALE and ALD dates back to the 1970s in Finland. The original pioneer of ALE was Tuomo Suntola, who demonstrated some of the first ALE processes as early as August/September 1974.[16] The first ALE system developed was ZnS.[16] The first ALE patent emerged in 1977.[17] The first literature paper on ALE appeared in 1980 in *Thin Solid Films*.[18] The first application of ALE was electroluminescent displays. The first public display of an ALE device was an electroluminescent display that operated in the Helsinki airport from 1983 to 1998. The first commercial ALE reactor was the F-120 sold by Microchemistry in 1988. The first of a series of ALE meetings was held in 1990 and continued through 1996. The first of a series of yearly ALD meetings was held in 2001 and has continued through the present date.

Many earlier reviews have addressed the basics of ALE or ALD.[5,8,11,12,19−21] Many previous reviews have considered the application of ALE or ALD to microelectronics and nanotechnology.[19,22−27] The intent of this present review is not to duplicate these previous reviews. Instead, this review is focused on an overview of key concepts and new directions in ALD. The semiconductor roadmap is coming to an end in a few years because of the limits of the current electronic materials. For continued progress, the future for electronic materials will embrace as yet undefined paradigms. ALD will almost certainly be part of the new paradigms because of its ability to control deposition on the atomic scale and to deposit conformally on very high aspect ratio structures.

2. Al_2O_3 ALD as a Model ALD System

The ALD of Al_2O_3 has developed as a model ALD system. An earlier extensive review by Puurunen has previously discussed the details of Al_2O_3 ALD.[20] Consequently, this section will only mention the highlights of Al_2O_3 ALD. Al_2O_3 ALD is usually performed using trimethylaluminum (TMA) and H_2O. The first reports of Al_2O_3 ALD using TMA and H_2O date back to the late 1980s and early 1990s.[28,29] More recent work in the semiconductor industry is using TMA and ozone for Al_2O_3 ALD.[30,31] This review will concentrate on Al_2O_3 ALD using TMA and H_2O.

The surface chemistry during Al_2O_3 ALD can be described as[5,14,32]

$$\text{(A) } \mathrm{AlOH^*} + \mathrm{Al(CH_3)_3} \rightarrow \mathrm{AlOAl(CH_3)_2^*} + \mathrm{CH_4} \quad (1)$$

$$\text{(B) } \mathrm{AlCH_3^*} + \mathrm{H_2O} \rightarrow \mathrm{AlOH^*} + \mathrm{CH_4} \quad (2)$$

where the asterisks denote the surface species. The Al_2O_3 ALD growth occurs during alternating exposures to TMA and H_2O. Al_2O_3 ALD is a model system because the surface reactions are very efficient and self-limiting. The main driver for the efficient reactions is the formation of a very strong Al−O bond. The overall reaction for Al_2O_3 ALD is

$$2\mathrm{Al(CH_3)_3} + 3\mathrm{H_2O} \rightarrow \mathrm{Al_2O_3} + 3\mathrm{CH_4} \qquad \Delta H = -376 \text{ kcal} \quad (3)$$

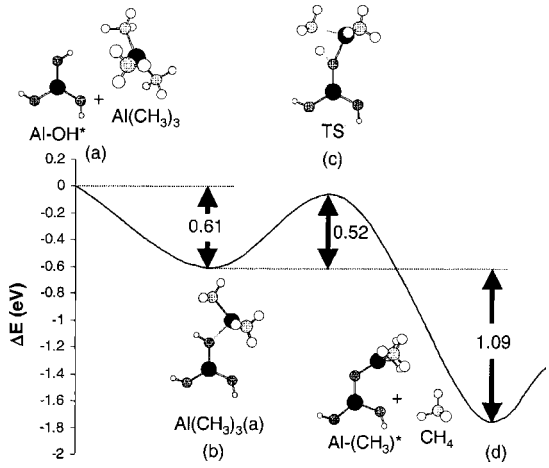

Figure 2. Reaction path and predicted energetics for reactions of $Al(CH_3)_3$ on the Al−OH* surface site calculated using the $Al(OAl(OH)_2)_2$−OH cluster. The structures are shown using the $Al(OH_2)$−OH cluster for clarity. (Reprinted with permission from ref 34. Copyright 2002 American Institute of Physics.)

This reaction has an extremely high reaction enthalpy.[33] This is one of the highest reaction enthalpies encountered for any ALD reaction.

The potential energy surfaces during Al_2O_3 ALD have been modeled using density functional theory (DFT).[34] These calculations show that $Al(CH_3)_3$ exists in a deep precursor well complexed to AlOH* species prior to its surface reaction, as shown in Figure 2.[34] Likewise, the calculations show that H_2O is also in a deep precursor well complexed to $AlCH_3$* species prior to its surface reaction. These complexes result from strong Lewis acid−base interactions on the surface. Although these precursor wells have not been experimentally observed, they may be fairly general for various classes of ALD reactions.

The surface chemistry of Al_2O_3 ALD has been confirmed by in situ FTIR studies.[32,35,36] The FTIR difference spectra clearly show the loss of AlOH* species and concurrent gain of $AlCH_3$* species during the TMA reaction. Likewise, the loss of $AlCH_3$* species and the concurrent gain of AlOH* species is observed during the H_2O reaction. The gas phase reaction products during Al_2O_3 ALD have also been identified using quadrupole mass spectrometry studies.[37,38] Using $Al(CH_3)_3$ and D_2O as the reactants, CH_3D was observed as the main reaction product, as expected from the surface chemistry for Al_2O_3 ALD.[37]

By repeating the surface reactions, Al_2O_3 growth is extremely linear with the number of AB cycles.[14,39] Various techniques, such as spectroscopic ellipsometry and quartz crystal microbalance (QCM) measurements, have characterized the growth per cycle during Al_2O_3 ALD. Typical measured Al_2O_3 ALD growth rates are 1.1−1.2 Å per AB cycle.[14,39] The resulting Al_2O_3 ALD films are smooth and extremely conformal to the underlying substrate. Studies on nanoparticles show excellent conformality of Al_2O_3 ALD films.[35,40,41] Investigations on high aspect ratio trench substrates also reveal superb conformality, as illustrated by the cross-sectional scanning electron microscopy (SEM) image in Figure 3.[42]

One of the hallmarks of ALD is self-limiting surface chemistry. The self-limiting surface reactions during Al_2O_3 ALD have been observed by in situ FTIR[32,35] and QCM[39] investigations as well as by spectroscopic ellipsometry studies.[14] The reactant exposures required for the surface

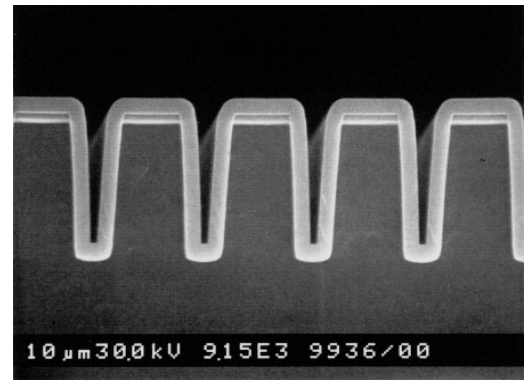

Figure 3. Cross-sectional SEM image of an Al_2O_3 ALD film with a thickness of 300 nm on a Si wafer with a trench structure. (Reprinted with permission from ref 42. Copyright 1999 John Wiley & Sons.)

reactions to reach completion reveal that the reactive sticking coefficients during Al_2O_3 ALD are much less than unity. Based on required exposure times, the reactive sticking coefficients are in the range of $\sim 10^{-3}-10^{-4}$ during Al_2O_3 ALD.[14]

The growth per one ALD cycle is also much smaller than one Al_2O_3 "monolayer". The growth rates of 1.1−1.2 Å per AB cycle can be compared with the thickness of one Al_2O_3 "monolayer". This monolayer thickness is estimated using the density of 3.0 g/cm^3 for Al_2O_3 ALD films grown at 177 °C.[43] Based on this density, the number density of "Al_2O_3" units is $\rho = 1.77 \times 10^{22}$ Al_2O_3 units/cm^3. The number of Al_2O_3 units per square centimeter is equal to $\rho^{2/3} = 6.8 \times 10^{14}$ cm^{-2}. Likewise, the monolayer thickness is equal to $\rho^{-1/3} = 3.8$ Å. The growth per AB cycle of 1.1−1.2 Å per AB cycle is much less than this estimate of the monolayer thickness.

The disagreement between growth per AB cycle and the monolayer thickness is not surprising because ALD growth is dependent on surface species and surface chemistry. This surface chemistry is not required to always yield a "monolayer" of growth during every AB cycle. The correlation between ALD growth and surface chemistry is clearly illustrated by the temperature-dependence of Al_2O_3 ALD growth per AB cycle. The growth per AB cycle decreases progressively with temperature between 177 and 300 °C. This decrease results from the progressive loss of AlOH* and $AlCH_3$* surface species at higher temperatures.[14,32]

The continuous and pinhole-free nature of Al_2O_3 ALD films is revealed by their superb electrical properties. Current−voltage curves for various Al_2O_3 ALD film thicknesses on n-Si(100) reveal electrical behavior that is very similar to that of thermal SiO_2 films.[7] The Al_2O_3 ALD films have a dielectric constant of ~7 and display very low electron leakage.[7] Increases in the current density versus applied potential occur as a result of Fowler−Nordheim tunneling. This characteristic is consistent with the absence of any defects or pinholes in the Al_2O_3 ALD film. These excellent properties have enabled Al_2O_3 ALD films to serve as gate oxides and to passivate semiconductor surfaces.[44−46]

3. Thermal and Plasma or Radical-Enhanced ALD

3.1. Thermal ALD

ALD is closely related to chemical vapor deposition (CVD) based on binary reactions such as A + B → Product.

For CVD using binary reactions, the A and B reactants are present at the same time and form the product film continuously on the substrate. In ALD, the substrate is exposed to the A and B reactants individually and the product film is formed in a stepwise and very digital fashion. A generic recipe for ALD is to find a CVD process based on a binary reaction and then to apply the A and B reactants separately and sequentially in an ABAB... binary reaction sequence.

There are many examples of ALD resulting from binary reaction CVD processes. Examples for TiO_2 and ZnO are based on the following binary CVD reactions and their corresponding reaction enthalpies:[33]

$$\text{TiO}_2\text{ ALD:}\quad \text{TiCl}_4 + 2\text{H}_2\text{O} \rightarrow \text{TiO}_2 + 4\text{HCl} \qquad \Delta H = -16\text{ kcal} \quad (4)$$

$$\text{ZnO ALD:}\quad \text{Zn(CH}_2\text{CH}_3)_2 + \text{H}_2\text{O} \rightarrow \text{ZnO} + 2\text{C}_2\text{H}_6 \qquad \Delta H = -70\text{ kcal} \quad (5)$$

These ALD systems yield a growth per AB cycle of ~0.4 Å from 150 to 600 °C for TiO_2 ALD[47] and 2.2−2.5 Å from 100 to 160 °C for ZnO ALD.[48,49] These ALD chemistries have negative heats of reaction and are robust ALD reactions. These reactions occur spontaneously at various temperatures and will be referred to as thermal because they can be performed without the aid of plasma or radical assistance.

A survey of developed ALD processes reveals that most thermal ALD systems are binary compounds based on binary reactant CVD.[20,21] The most common thermal ALD systems are binary metal oxides such as Al_2O_3, TiO_2, ZnO, ZrO_2, HfO_2, and Ta_2O_5. Other common thermal ALD systems are binary metal nitrides such as TiN, TaN, and W_2N. Thermal ALD systems also exist for sulfides such as ZnS and CdS and phosphides such as GaP and InP.

3.2. Plasma or Radical-Enhanced ALD

There is also a need for single-element ALD materials, such as metals and semiconductors, that can be deposited using a binary reaction sequence. Except for some notable exceptions discussed in section 5, the single-element films of metals and semiconductors are very difficult to deposit using thermal ALD processes. Fortunately, these single-elements can be deposited using plasma or radical-enhanced ALD.[22] The radicals or other energetic species in the plasma help to induce reactions that are not possible using just thermal energy. Plasma sources can be used to generate hydrogen radicals that reduce the metal or semiconductor precursors. Hydrogen radicals can also be produced using a hot tungsten filament. A scheme for metal ALD using metal reactants and hydrogen radicals is shown in Figure 4.

Hydrogen radical-enhanced ALD was first demonstrated for Ti ALD[50] using a H_2 plasma. Ta ALD is another ALD system that has been studied extensively using hydrogen radicals from H_2 plasmas.[51] The reactants for Ta ALD are $TaCl_5$ and hydrogen radicals.[51] The surface chemistry for Ta ALD can be expressed as

$$\text{(A) Ta*} + \text{TaCl}_5 \rightarrow \text{TaTaCl}_5\text{*} \quad (6)$$

$$\text{(B) TaCl}_5\text{*} + 5\text{H}\cdot \rightarrow \text{Ta*} + 5\text{HCl} \quad (7)$$

$TaCl_5$ is first exposed to the surface. Subsequently, the hydrogen radicals reduce the Ta atoms and remove the chlorine from the surface. Although the growth per cycle during Ta ALD is only 0.08 Å per AB cycle, the Ta ALD films have excellent film resistivities and show good Cu barrier properties.[51] The small growth per cycle is attributed to steric hindrance caused by the large $TaCl_5$ admolecule on the surface. XRD also indicates that the Ta ALD film is β-Ta and has very small nanograins.[51]

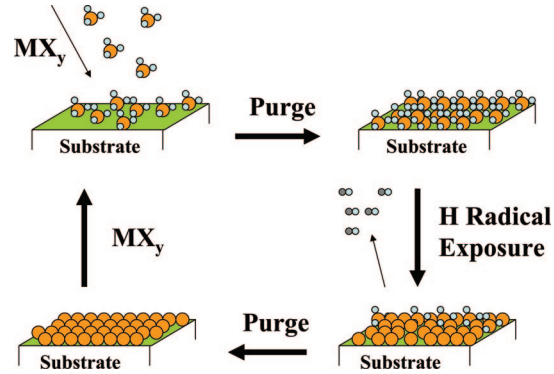

Figure 4. Schematic diagram of hydrogen radical-enhanced ALD using a metal reactant and hydrogen radicals.

The limitations of hydrogen radical-enhanced ALD were also demonstrated by studies using trenched samples.[51] The Ta ALD films were not conformal in trenches with a high aspect ratio of 40:1. When the Ta ALD film had a thickness of 28 nm at the top of the trench, the thickness was only 11 nm at the bottom of the trench. The lower Ta ALD growth at the bottom of the trench is attributed to hydrogen radical recombination on the walls of the trench that attenuates the hydrogen radical flux.[52] Radical recombination will limit the general utility of plasma ALD in high aspect ratio structures.

The ALD of single-element semiconductors such as Si and Ge can also be deposited using hydrogen radical-enhanced ALD. The surface chemistry for Si ALD is based on the desorption kinetics for H_2, HCl, and $SiCl_2$ from silicon surfaces. H_2 desorbs at 535 °C,[53,54] HCl desorbs at 575 °C,[53] and $SiCl_2$ desorbs at 725 °C[53,55] during temperature programmed desorption (TPD) experiments from silicon surfaces. H_2 desorbs at a lower temperature than HCl from silicon surfaces. $SiCl_2$ desorbs at a higher temperature than HCl from silicon surfaces. Consequently, silicon can be deposited using a chlorine-containing silicon precursor such as SiH_2Cl_2.

The surface chemistry for Si ALD using SiH_2Cl_2 and hydrogen radicals can be written as

$$\text{(A) Si*} + \text{SiH}_2\text{Cl}_2 \rightarrow \text{SiSiCl}_2\text{*} + \text{H}_2 \quad (8)$$

$$\text{(B) SiCl}_2\text{*} + 2\text{H} \rightarrow \text{Si*} + 2\text{HCl} \quad (9)$$

At the appropriate temperature, H_2 and HCl will desorb upon SiH_2Cl_2 adsorption but $SiCl_2$ will not desorb from the silicon surface. The build up of chlorine on the silicon surface will produce a self-limiting adsorption of SiH_2Cl_2. The surface chlorine can then be removed by exposing the surface to hydrogen radicals. The hydrogen radicals add hydrogen atoms to the silicon surface that recombine with surface chlorine to desorb as HCl or with other surface hydrogen atoms to desorb as H_2. The hydrogen radical flux will eventually remove all the surface chlorine species.

Studies of Si ALD using SiH_2Cl_2 and H radicals have demonstrated the self-limiting nature of Si ALD growth versus both SiH_2Cl_2 and hydrogen radical exposures.[56,57] A Si ALD growth per cycle of ~1.6 Å was observed between

550 and 610 °C. At higher temperatures, the Si ALD growth per cycle increased as a result of Si CVD. At lower temperatures, the Si ALD growth per cycle decreased as a result of incomplete surface reactions. A similar strategy was also applied for Ge ALD using GeH_2Cl_2 and hydrogen radicals.[58,59]

Si and Ge ALD were both demonstrated on silicon and germanium surfaces. However, a difficulty with Si and Ge ALD is their nucleation on other types of surfaces. Si and Ge are both very reactive and easily react with oxygen from oxide substrates to form SiO_2 or metals from metallic substrates to form silicides. Consequently, the nucleation of Si and Ge ALD is very difficult. The nucleation problems have limited the surface chemistry for Si and Ge ALD to only silicon and germanium surfaces.

In addition to single-element materials, plasma-enhanced ALD can deposit compound materials. One important advantage is that plasma-enhanced ALD can deposit films at much lower temperatures than thermal ALD. For example, plasma-enhanced Al_2O_3 ALD can be performed using TMA and O_2 plasma at temperatures as low as room temperature.[60] The low temperature deposition is useful for coating thermally fragile substrates such as polymers.[61] The plasma-enhanced Al_2O_3 ALD films also have improved electrical properties compared with thermal Al_2O_3 ALD[62] and lead to excellent passivation of silicon substrates.[63]

Plasma-enhanced ALD has also been useful to deposit metal nitrides, such as TiN and TaN, which generally cannot be grown with high quality using organometallic precursors.[64] TaN ALD has been achieved using organometallic tantalum precursors such as terbutylimidotris(diethylamido)tantalum (TBTDET) and hydrogen radicals.[60,65,66] The plasma-enhanced process can form TaN films that have much lower electrical resistivity and higher density than TaN ALD films grown using thermal TaN ALD with TBTDAT and NH_3.[67,68]

Oxygen radical-enhanced ALD has been employed to grow metal oxides using metal β-diketonate precursors. Metal oxides, such as Y_2O_3, have been grown at low temperatures with minimal carbon contamination.[69] Remote O_2 plasmas have also been utilized for plasma enhanced Pt ALD with (methylcyclopentadienyl)trimethylplatinum as the metal precursor.[70] In addition, plasma-enhanced Ru ALD has been accomplished using bis(ethylcyclopentadienyl)ruthenium and NH_3 plasma.[71] These plasma-enhanced Ru ALD films have potential as adhesion layers for copper interconnects.[65]

4. Reactors for ALD

There are different types of ALD reactors. Many ALD reactor designs were discussed in the original patents by T. Suntola in 1977[17] and 1983.[72] Various ALD reactors and design principles were also described in early reviews of ALE by T. Suntola.[12,13,73] One of the early ALD reactors had a revolving substrate holder that rotated the substrate in and out of the A and B reactant flow streams. Another design was based on gas flow through hot wall CVD tube reactors. Other ALD reactors flowed the reactant in an inert carrier gas through a small channel between the reactor wall and substrate. This design was known as the "traveling-wave" reactor and is represented by the F-120 reactor by Microchemistry Ltd.[11]

To organize the various ALD reactor designs, there are two limiting types of ALD reactors that can be defined by the pumping and use of a carrier gas. In one limit are ALD reactors where the reactants are exposed without using a carrier gas and sometimes with throttled pumping.[14,15,74] After the exposures, the reactants are removed by opening up completely to the pump and evacuating the reactor. Because of the long residence times in the reactor, these exposures can utilize reactants very efficiently. However, the evacuation times for these ALD reactors can be slow in the absence of a purge gas. At low pressures in molecular flow, the random walk of molecules colliding only with the reactor walls leads to long pumping times.

In another limit are ALD reactors where the reactants are exposed with a carrier gas flowing through the reactor.[12,39,75] The carrier gas is in viscous flow and flows continuously to the pump. If the reactants have sufficient vapor pressure, the reactants can be dosed into the carrier gas stream. Alternatively, the carrier gas can flow over the headspace of a solid or liquid reactant or through the liquid reactant if the reactant has a lower vapor pressure. The carrier gas entrains the reactants and products and defines a short residence time in the reactor. The advantage of the viscous flow reactors is their much shorter ALD cycle times relative to the ALD reactors employing no carrier gas during reactant exposure and purging.

Most ALD reactors operate with an inert carrier gas in viscous flow. The optimum pressure for viscous flow reactors is around ~1 Torr. This optimum pressure is a trade-off between gas interdiffusion and entrainment. For example, the interdiffusion coefficient of O_2 in N_2 is $D_{12} = 132$ cm^2/s at 1 Torr and 0 °C. This interdiffusion coefficient is determined knowing that $D_{12} = 0.174$ cm^2/s at 1 atm and 0 °C[76] and that gas diffusion is inversely proportional to pressure, $D \sim 1/P$.[76] The mean squared displacement, x^2, resulting from gas diffusion is $x^2 = 6Dt$, where t is time. Therefore, the mean displacement for O_2 in N_2 gas at 1 Torr and 0 °C is $x = 28$ cm in 1 s. This sizable mean displacement indicates that diffusion of reactants in N_2 gas at 1 Torr is sufficient for removal of reactants and products from stagnant gas in the reactor in a reasonable time.

The pressure of 1 Torr is also high enough for the N_2 to be an effective carrier gas. The mean free path, λ, between N_2 molecules at room temperature is $\lambda \sim 5 \times 10^{-3}$ cm/P, where P is in Torr.[77] This approximation reveals that the mean free path of N_2 at 1 Torr is $\lambda \sim 50$ μm. This small mean free path indicates that N_2 gas is in viscous flow at 1 Torr and will effectively entrain reactants. Mean displacements may be too small for effective purging from stagnant gas at pressures higher than 1 Torr. Entrainment will be less effective at pressures lower than 1 Torr when the gas mean free paths are longer. Inert carrier gas pressures around ~1 Torr are a compromise between these two factors.

One ALD reactor that optimizes the residence times during reaction and purging is known as synchronously modulated flow and draw (SMFD).[78] The SMFD design injects the inert flowing gas at the reactor inlet during the purge steps and at the reactor outlet during the reactant exposures. The synchronized modulation of the inert flowing gas between the reactor inlet and the reactor outlet enables high-speed gas flow switching. A schematic illustrating the dose and purge modes during SMFD is shown in Figure 5.[79]

The reactant has a long residence time during dosing and only experiences a slow "draw" from the inert flowing gas entering at the reactor outlet. The reactant can be utilized very efficiently during the dose mode. In contrast, the reactant has a short residence time during the purge mode because inert carrier gas enters at the reactor inlet and flows through

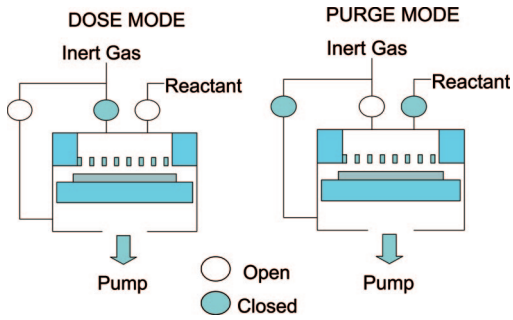

Figure 5. Illustration of purge and dose modes during synchronous modulation of flow and draw. (Adapted from information provided by Sundew Technologies, LLC.)

the reactor. The SMFD design leads to short ALD cycle times of <1 s for ALD systems such as Al_2O_3 ALD.[79]

Single-wafer ALD reactors for semiconductor processing may have different configurations for the gas flow. The "cross-flow" reactors have parallel gas flows across the wafer surface. The "showerhead" reactors bring the gas into the reactor perpendicular to the wafer surface through a distributor plate. The gas then flows radially across the wafer surface. Other distinctions between ALD reactors are between hot and cold wall reactors. In "hot wall" reactors, the walls, gas, and substrates in the reactor are all heated to the temperature of the walls. In "cold wall" reactors, only the substrate is heated and the walls remain at room temperature or are only warmed slightly.

Other ALD reactors can deposit on many samples simultaneously. These reactors are known as "batch" reactors. They can coat multiple samples at the same time and can dramatically shorten the required time to coat one sample. The batch reactors can improve the cost and time effectiveness for commercial ALD processes. Reactant and purging time constants are longer in batch reactors because of larger reactor volumes and lower gas conductance between multiple samples. However, the multiplex advantage can offset the longer time constants.

Plasma reactant sources have also become increasingly important for ALD processing. Inductively coupled plasma (ICP) is a common plasma source during plasma ALD. Plasmas usually operate at pressures of ~100−500 mTorr.

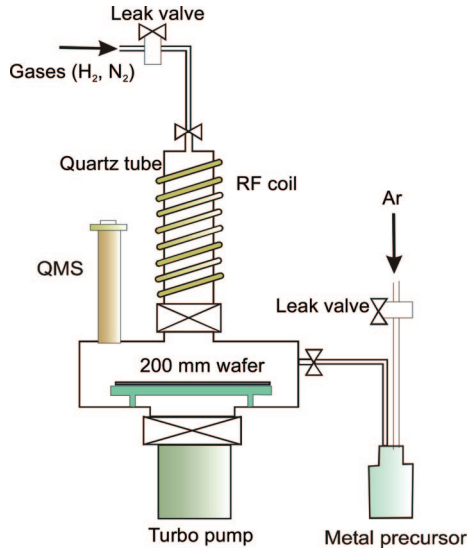

Figure 6. Schematic diagram of a plasma-enhanced ALD system used for Ta ALD and Ti ALD. (Reprinted with permission from ref 51. Copyright 2002 American Institute of Physics.)

Plasma-enhanced ALD is not performed with an inert carrier gas during the plasma reaction cycle. However, the plasma reaction cycle may alternate with a conventional reactant ALD cycle using an inert carrier gas. The plasma ALD reactor used for Ta ALD[51] and Ti ALD[50] is shown in Figure 6. A commercial plasma ALD reactor for 200 mm wafers was also recently described for TiN and HfO_2 ALD.[80]

5. Metal ALD Using Thermal Chemistry

Metal ALD can also be accomplished using thermal chemistry without the aid of plasma or radical assistance.[22] Thermal chemistry for metal ALD is very important because thermal chemistry does not have the limitations caused by surface recombination that restrict radical-enhanced ALD in high aspect ratio structures. Metal ALD based on thermal chemistry has been demonstrated for a variety of metals. There are three main types of metal ALD using thermal chemistry that have been successful. These ALD surface chemistries are based on fluorosilane elimination, combustion chemistry, or hydrogen reduction.

5.1. Fluorosilane Elimination Chemistry

Fluorosilane elimination reactions result from the reaction of metal fluorides and silicon precursors such as SiH_4 and Si_2H_6. These reactions were first demonstrated for W ALD.[81] The basis for these reactions is the formation of a very stable Si−F bond that leads to a very exothermic reaction. The overall chemistry for W ALD using WF_6 and Si_2H_6 is[33]

$$WF_6 + Si_2H_6 \rightarrow W + SiF_3H + 2H_2 \qquad \Delta H = -181 \text{ kcal} \quad (10)$$

Other metals can also be deposited using fluorosilane elimination reactions such as Mo ALD according to[33]

$$MoF_6 + Si_2H_6 \rightarrow Mo + SiF_3H + 2H_2 \qquad \Delta H = -220 \text{ kcal} \quad (11)$$

The high reaction enthalpies of $\Delta H = -181$ kcal for W ALD and $\Delta H = -220$ kcal for Mo ALD are comparable to or higher than the reaction enthalpy of $\Delta H = -376$ kcal for Al_2O_3 ALD on a per mole of metal basis.

The surface chemistry during W ALD using WF_6 and Si_2H_6 as the reactants can be simply expressed as[81,82]

$$\text{(A) } WSiF_2H^* + WF_6 \rightarrow WWF_5^* + SiF_3H \quad (12)$$

$$\text{(B) } WF_5^* + Si_2H_6 \rightarrow WSiF_2H^* + SiF_3H + 2H_2 \quad (13)$$

This surface chemistry is supported by in situ FTIR studies of the absorbance from Si−H and W−F stretching vibrations on surface species during the WF_6 and Si_2H_6 exposures.[81] The absorbance from Si−H stretching vibrations decreases and the absorbance from W−F stretching vibrations increases concurrently during WF_6 exposures. The absorbance from W−F stretching vibrations decreases and the absorbance from Si−H stretching vibrations also increases concurrently during Si_2H_6 exposures.

The surface chemistry for W ALD leads to the linear deposition of W ALD films versus AB cycles, as shown in Figure 7.[83] QCM studies have measured W ALD growth per cycle, which varies from 4 to 7 Å versus surface temperatures

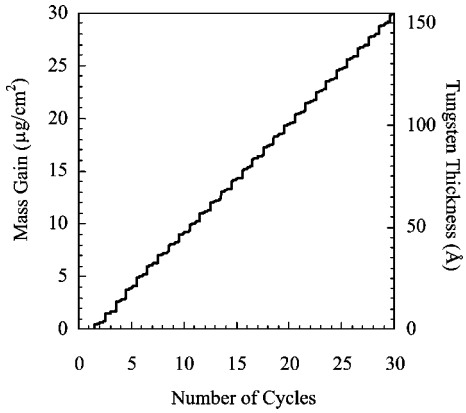

Figure 7. Mass gain monitored by quartz crystal microbalance for 30 cycles during W ALD using WF_6 and Si_2H_6 as the reactants. The corresponding tungsten thickness has been calculated assuming a density of 19.3 g/cm^3. (Reprinted with permission from ref 83. Copyright 2005 Elsevier.)

from 177 to 325 °C and Si_2H_6 reactant exposures from $\sim 10^4$ to 10^6 Langmuirs.[83] The dependence on surface temperature and Si_2H_6 exposure is believed to be caused by Si_2H_6 insertion into Si−H bonds.[83,84] This bond insertion mechanism leads to a Si CVD contribution to the W ALD growth. The Si CVD contributions are more pronounced at higher temperatures and larger Si_2H_6 exposures.[84] W ALD is used during semiconductor fabrication as a nucleation layer for tungsten plug fill processes.[85]

5.2. Combustion Chemistry

Some catalytic metals can be deposited using combustion chemistry. In this process, the organic ligands of the organometallic metal precursors react with oxygen to produce CO_2 and H_2O as combustion products. Ru and Pt were the first metal ALD systems that were deposited using combustion chemistry.[86,87] The Ru precursor was $Ru(C_5H_5)_2$ (bis(cyclopentadienyl)ruthenium), and the Pt precursor was $(CH_3C_5H_4)Pt(CH_3)_3$ ((methylcyclopentadienyl)trimethylplatinum). The oxygen precursor was O_2. Ru ALD was accomplished at temperatures between 275 and 400 °C, and the growth per cycle was 0.4−0.5 Å at 350−400 °C.[86] Pt ALD was initially reported at 300 °C, and the growth per cycle was also 0.4−0.5 Å.[87]

The mechanism of Ru ALD and Pt ALD was explored using quadrupole mass spectrometry (QMS) and QCM studies.[88] The QMS investigations observed H_2O and CO_2 during both the organometallic precursor and O_2 exposures. These classic combustion products suggest an overall reaction for Ru ALD of

$$Ru(Cp)_2 + {}^{25}/_2O_2 \rightarrow Ru + 10CO_2 + 5H_2O \quad (14)$$

The individual surface chemical reactions for Ru ALD are proposed to be

$$(A)\ RuO_x^* + Ru(Cp)_2 \rightarrow RuRu(Cp)^* + 5CO_2 + {}^5/_2H_2O \quad (15)$$

$$(B)\ RuCp^* + yO_2 \rightarrow RuO_x^* + 5CO_2 + {}^5/_2H_2O \quad (16)$$

The QCM studies are especially interesting because they reveal large mass gains during the O_2 exposures, as displayed in Figure 8.[88] The oxidation of surface organic species initially produces a mass loss. A subsequent mass gain is produced when O_2 deposits oxygen to the Ru surface and the subsurface region. This surface oxygen is then available to oxidize some of the incoming organic ligands on the organometallic precursor.

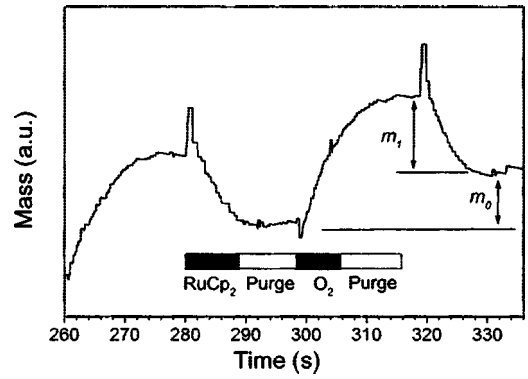

Figure 8. Quartz crystal microbalance data measured during the reaction cycles for Ru ALD using $RuCp_2$ and oxygen as the reactants. (Reprinted with permission from ref 88. Copyright 2003 The Electrochemical Society.)

This combustion chemistry is believed to occur most easily for group VIII metals that are known to be heterogeneous catalysts. The ALD of other catalytic metals such as Ir[89] and Rh[90] has also been demonstrated using combustion chemistry. These metal ALD systems are being explored by the semiconductor industry. Ruthenium is under consideration as a seed for Cu electrodeposition for backend interconnects.[91] Ru ALD is a possible seed for Cu deposition in part because of the lattice match between the stable hexagonal plane of Ru(001) and the closed-packed face-centered cubic Cu(111) plane.[92]

5.3. Hydrogen Reduction Chemistry

There have also been attempts to develop metal ALD based on various organometallic precursors and H_2 reduction. The first efforts focused on Cu ALD using CuCl and H_2 as the reactants.[93] Copper films were reported to be grown on tantalum substrates.[93] However, CuCl is problematic as a copper source.[94] Additional studies explored Cu ALD using Cu(II)-2,2,6,6-tetramethyl-3,5-heptanedionate ($Cu(thd)_2$) and H_2 as the reactants.[95] Area-selective ALD was achieved on platinum seeded substrates.[95]

Cu ALD has also been accomplished using another copper β-diketonate, Cu(II) 1,1,1,5,5,5-hexafluoroacetylacetonate ($Cu(hfac)_2$), and various organic reduction agents such as methanol, ethanol, and fomalin.[96,97] Very good conformal Cu ALD films were reported on trenched substrates.[96,97] The ALD of other metals has also been demonstrated using organic reducing agents. Pd ALD has been demonstrated using $Pd(hfac)_2$ and formalin.[98] H_2 was also reported to be effective as the reducing agent for Pd ALD after the nucleation of the Pd ALD films using formalin as the reducing agent.[98]

Alternative approaches to metal ALD have focused on depositing a metal oxide and then reducing this metal oxide with H_2 or other reducing agents. This method circumvents the fairly unreactive metal surface following H_2 reduction. During metal oxide ALD, there is an oxide or M−OH species on the surface to react with the organometallic precursor. This approach has been demonstrated for the growth of NiO

films using Ni acetylacetonate ($Ni(acac)_2$) and O_3 and the subsequent reduction to Ni films using H_2.[99] A similar technique was developed using bis(cyclopentadienyl)nickel and H_2O as the reactants for NiO growth and then hydrogen radicals for the reduction to Ni metal.[100] In addition, there are continued efforts to extend the range of metal precursors that will facilitate metal ALD using H_2 reduction chemistry. New families of metal precursors have been explored for metal ALD including the metal acetamidinates.[101]

6. Nucleation and Growth during ALD

The nucleation of ALD is extremely important for continuous and pinhole-free ultrathin films. If the ALD precursors do not effectively react with the initial substrate, then the ALD film may not nucleate at all or may nucleate only at particular defect sites on the initial substrate. This lack of uniform nucleation can produce island growth as described by a Volmer−Weber growth mechanism.[102] After multiple ALD cycles, the islands may grow together and form a continuous film. However, in the ultrathin film regime, the ALD films are rough and not conformal to the initial substrate.

6.1. Metal Oxide ALD on H−Si(100)

The lack of nucleation is very serious for the deposition of ultrathin dielectric films such as the high dielectric constant gate oxides in MOSFETs. These gate oxides need to be ultrathin and extremely conformal to ensure uniform electrical performance across the entire gate oxide. The nucleation of the high *k* gate oxides on the initial hydrogen-passivated Si(100) surfaces has been one of the most challenging nucleation problems for ALD. Many ALD nucleation studies have focused on this important technological problem.

Effective nucleation for ALD requires surface chemical species that will react with the ALD precursors. To obtain a uniform layer-by-layer ALD film growth as described by the Frank van der Merwe mechanism,[102] the ALD precursor needs to react with the initial surface species on the very first ALD cycle. This type of efficient nucleation is observed for metal oxide ALD on oxide substrates and usually for metal nitride ALD on oxide substrates. Oxide surfaces have MOH* hydroxyl groups that are typically reactive with organometallic precursors. The organometallic precursors are also usually reactive with H_2O and NH_3 that are commonly employed for metal oxide and metal nitride ALD, respectively.

Inefficient ALD nucleation is observed for metal oxide ALD on hydrogen-passivated Si(100) surfaces (H−Si(100)). The nucleation of ZrO_2 ALD and HfO_2 ALD has been reported on H−Si(100) because of the importance of these high dielectric constant materials as replacements for the thermal SiO_2 on Si(100) in MOSFETS.[103] Rutherford backscattering spectroscopy (RBS) was used to measure the ZrO_2 thickness on H−Si(100) surfaces as a function of the number of ALD cycles during ZrO_2 ALD using $ZrCl_4$ and H_2O as the precursors.[103] The RBS measurements indicated that the ZrO_2 ALD film did not nucleate and achieve a linear growth per cycle until after 50−60 ALD cycles. Transmission electron microscopy (TEM) analysis also revealed that the ZrO_2 ALD films were very granular with distinct islands for nucleation on the H−Si(100) surface.[104] In contrast, the ZrO_2 ALD film nucleated efficiently and formed a very smooth and conformal film on an oxidized Si(100) surface.[104]

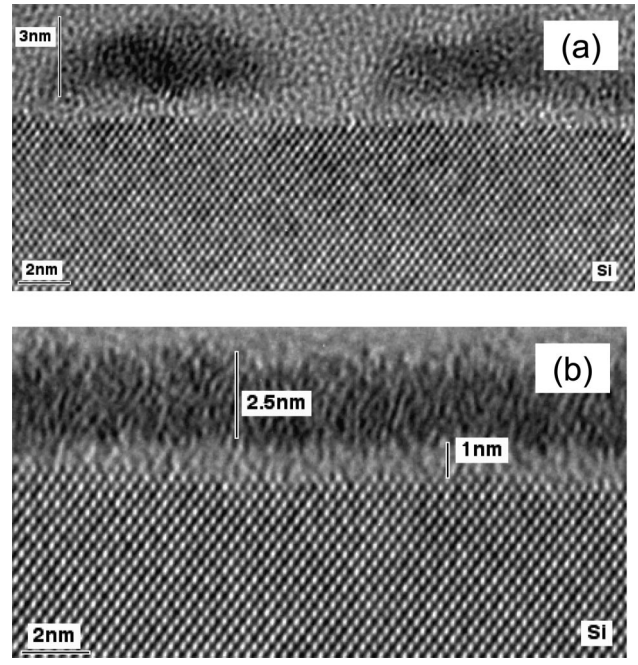

Figure 9. (a) Cross-section TEM image of a HfO_2 ALD film deposited on a Si wafer immediately after HF-last surface treatment. (b) Cross-section TEM image of a HfO_2 ALD film deposited on a SiO_2 layer on a Si wafer. (Reprinted with permission from ref 106. Copyright 2003 Elsevier.)

Similar results were obtained for the nucleation and growth of HfO_2 ALD on H−Si(100) surfaces. RBS measurements revealed that the HfO_2 ALD did not achieve a linear growth per cycle until after 25−30 ALD cycles using $HfCl_4$ and H_2O as the precursors.[105] Alternatively, a variety of oxides on Si(100) produced by chemical treatment or rapid thermal oxidation displayed very rapid nucleation and nearly linear HfO_2 ALD growth from the very first ALD cycle.[105] TEM measurements have captured the nonuniform islands of HfO_2 ALD on the initial H−Si(100) surface as shown in Figure 9a and the conformal HfO_2 ALD film on the oxide on the initial Si(100) surface as displayed in Figure 9b.[106] These studies reveal that a thin oxide coating is required for the efficient nucleation of ZrO_2 or HfO_2 ALD on Si(100). This SiO_2 coating must be kept ultrathin to avoid the effects of the lower SiO_2 dielectric constant on the gate stack.

Al_2O_3 ALD also displayed nucleation difficulties on H−Si(100).[103] Measurements of the Al_2O_3 ALD film thickness versus number of ALD cycles indicated that 10−15 ALD cycles were required to obtain a linear growth per cycle.[103] These studies were performed using $Al(CH_3)_3$ and H_2O as the ALD precursors. Additional studies investigated the mechanism of Al_2O_3 ALD on H−Si(100) using in situ Fourier transform infrared (FTIR) studies.[107,108] H_2O did not react with the H−Si(100) surface even after extremely large H_2O exposures. There was evidence for some reactivity of $Al(CH_3)_3$ or $Al(CH_3)OH$ with the H−Si(100) surface. The H_2O could then react with $AlCH_3$* surface species and progressively nucleate Al_2O_3 ALD on the H−Si(100) surface.

6.2. Metal ALD on Oxide Surfaces

Metal ALD on oxide surfaces is another ALD system that displays nucleation difficulties. This nucleation problem is not surprising, since metals do not generally wet oxide surfaces. Many studies in heterogeneous catalysis indicate that metals prefer to form clusters on oxide surfaces. W ALD

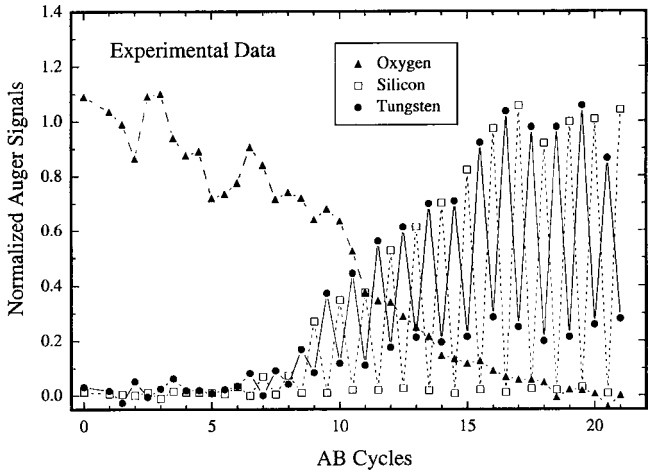

Figure 10. Normalized Auger electron spectroscopy (AES) signals versus AB cycles during W ALD on a SiO_2 surface using WF_6 and Si_2H_6 as the reactants. The AES signals at integer AB cycle numbers were recorded after the Si_2H_6 exposures. (Reprinted with permission from ref 109. Copyright 2001 Elsevier.)

using WF_6 and Si_2H_6 as the reactants has been studied thoroughly to understand the nucleation mechanism on SiO_2 and Al_2O_3 substrates. Auger electron spectroscopy (AES) investigations have shown that W ALD requires approximately 8−9 cycles to nucleate on SiO_2 surfaces[109] and approximately 3−4 cycles on Al_2O_3 surfaces.[110] The AES results for W ALD nucleation on SiO_2 surfaces are shown in Figure 10.[109] The nucleation period can be shortened to 4−5 cycles for W ALD on SiO_2 by much larger Si_2H_6 exposures on the first ALD cycle. Likewise, the nucleation is also facilitated by electron beam irradiation of the Al_2O_3 surface.[109]

The nucleation of W ALD on Al_2O_3 is important in the growth of precise W/Al_2O_3 nanolaminates using W ALD and Al_2O_3 ALD. QCM investigations have observed the nucleation delay for W ALD on Al_2O_3. The nucleation of W ALD on the Al_2O_3 ALD surface is observed to require 3−4 cycles using larger Si_2H_6 exposures, in good agreement with the AES investigations.[111] In addition, the growth per cycle during the W ALD nucleation provides evidence for an island growth mechanism.[111]

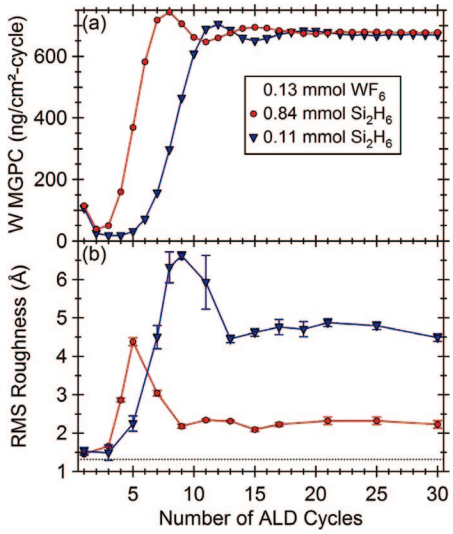

Figure 11. (a) W ALD mass gain per cycle and (b) root-mean-squared (rms) roughness for W ALD on a hydroxylated Al_2O_3 surface at 122 °C for WF_6 reactant exposure of 0.13 mmol and two different Si_2H_6 exposures of 0.11 and 0.83 mmol. (Reprinted with permission from ref 114. Copyright 2009 American Institute of Physics.)

The W ALD growth per cycle is initially very small during the first several W ALD cycles. The W ALD growth per cycle then increases dramatically and reaches a maximum before reducing to a slightly smaller W ALD growth per cycle. This behavior is expected as W ALD islands grow and then grow together and coalesce to form a continuous film.[112,113] More recent studies have also observed that the roughness of the W ALD surface is highest in the region where the islands are initially growing rapidly prior to reaching the maximum W ALD growth per cycle.[114] A correlation between the root-mean-square surface roughness measured by atomic force microscopy (AFM) and the W ALD growth per cycle is shown in Figure 11.[114]

6.3. Al_2O_3 ALD on Carbon Nanotubes and Graphene Surfaces

Another example of nucleation difficulty for ALD is Al_2O_3 ALD on carbon nanotubes (CNTs). The surface of the CNT is very inert and does not contain chemical species that allow for the reaction of either $Al(CH_3)_3$ or H_2O during Al_2O_3 ALD. As a result, Al_2O_3 ALD on single-walled and multiwalled CNTs yields only the growth of isolated Al_2O_3 nanospheres.[115,116] These nanospheres are believed to originate from specific defects on the surface of the CNTs. The nucleation of the Al_2O_3 ALD can be facilitated by the functionalization of the CNTs with nitroaniline or NO_2.[115−117] The NO_2 group on the surface of the CNTs provides a chemical site for the adsorption of $Al(CH_3)_3$ and yields a very conformal Al_2O_3 ALD film on the CNTs after multiple Al_2O_3 ALD cycles.

Nucleation difficulties are also encountered for ALD on graphene surfaces. Like the CNT surface, the graphene surface is inert. Al_2O_3 ALD and HfO_2 ALD have resulted in the growth of nanoribbons only along the step edges of the graphene surface.[118] The step edges are believed to serve as ALD nucleation sites.[118] Ozone has also been employed to create nucleation sites on the basal plane of graphene for Al_2O_3 ALD.[119] Chemical treatment using perylene tetracarboxylic acid has also been used to functionalize graphene for Al_2O_3 ALD.[120]

7. Low Temperature ALD

The ability to perform ALD at low temperatures is important to maintain a low thermal budget to prevent the interdiffusion of materials. This problem is particularly severe for nanostructured devices. Low temperature ALD is also needed for ALD on thermally fragile substrates such as polymeric or biological samples. Fortunately, several ALD systems can be performed at low temperatures because of their favorable thermochemistry. A few other special ALD systems can be facilitated to occur at much lower temperatures using a catalyst.

7.1. Al_2O_3 ALD and Other Metal Oxide ALD

The high exothermicity of the Al_2O_3 ALD surface reactions enables this ALD system to be performed at temperatures as low as room temperature.[43] QCM investigations have revealed that Al_2O_3 ALD can be grown over a wide range of temperatures with little change in the growth per cycle.[43] The Al_2O_3 ALD films do show a small decrease in

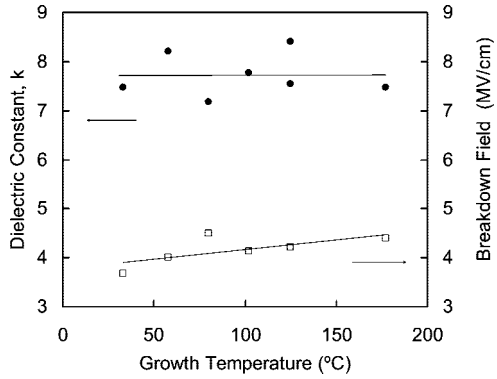

Figure 12. Dielectric constant and breakdown field of low-temperature Al_2O_3 ALD films grown using 300 AB cycles on n-Si(100). (Reprinted with permission from ref 43. Copyright 2004 American Chemical Society.)

density from 3.0 g/cm^3 at 177 °C to 2.5 g/cm^3 at 33 °C. In addition, the refractive index also decreases slightly, as expected from the reduction of the density. The quality of the Al_2O_3 ALD films is excellent over this entire temperature range.[43] XRR studies of the Al_2O_3 ALD films indicate that the films are very conformal to the initial substrate and display minimal surface roughness even for films deposited at 33 °C.

The major issue for Al_2O_3 ALD at low temperatures is the required purge times to avoid Al_2O_3 CVD. QCM studies have shown that the minimum purge times are 1 and 5 s after the $Al(CH_3)_3$ and H_2O exposures, respectively, at 177 °C.[43] These minimum purge times increased to 20 and 180 s after the $Al(CH_3)_3$ and H_2O exposures, respectively, at 33 °C.[43] The large increase in the purge time after the H_2O exposure results from the high desorption activation energy for H_2O from the surfaces of the ALD reactor. Slow H_2O desorption rates at low temperature lead to much longer required purge times to avoid Al_2O_3 CVD.

Forward recoil spectrometry of the Al_2O_3 ALD films has also revealed that the hydrogen atom % increases in Al_2O_3 ALD films grown at low temperatures.[43] The hydrogen atom % was ~6% for Al_2O_3 ALD films grown at 177 °C. The hydrogen atom % increased to ~22% for Al_2O_3 ALD films grown at 33 °C. Although the hydrogen atom % increased at lower temperatures, some of the electrical properties of the Al_2O_3 ALD films remained largely unchanged over the entire temperature range. The dielectric constant of the Al_2O_3 ALD films was constant at ~7−8, and the breakdown field was ~4 MW/cm from 33−177 °C, as shown in Figure 12.[43] Additional investigation of the Al_2O_3 ALD films is required to evaluate the fixed charge density and its dependence on the hydrogen atom %.

Several other ALD processes besides Al_2O_3 ALD have been demonstrated at low temperatures. These low temperature ALD systems have been reported in a recent review and are important for ALD on organic and biological substrates.[24] Some key ALD systems displaying growth at ≤100 °C are TiO_2 ALD using $TiCl_4$ and H_2O or $Ti(OiPr)_4$ and H_2O as the reactants[121,122] and ZnO ALD using $Zn(Et)_2$ and H_2O as the reactants.[123] These low temperature ALD systems enable ALD on polymers and ALD on organic and biological templates, as discussed in sections 8 and 13.

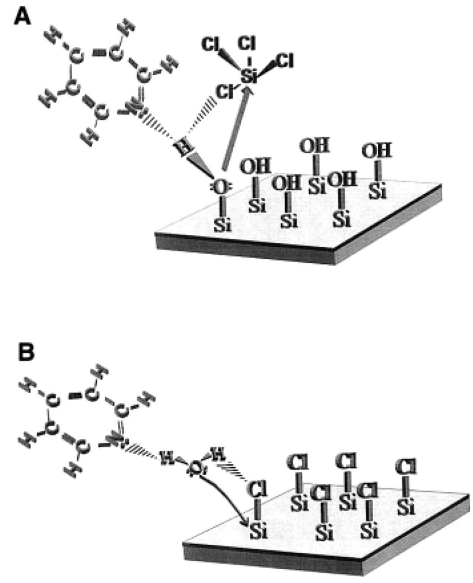

Figure 13. Proposed mechanism for Lewis base catalysis of SiO_2 ALD during (a) the $SiCl_4$ reaction and (b) the H_2O reaction. (Reprinted with permission from ref 127. Copyright 1997 American Association for the Advancement of Science.)

7.2. Catalytic SiO_2 ALD

The use of catalysts for gas phase deposition during ALD or CVD is very unusual. One ALD system that can be catalyzed is SiO_2 ALD using $SiCl_4$ and H_2O as the reactants. SiO_2 ALD is based on the binary reaction

$$SiCl_4 + 2H_2O \rightarrow SiO_2 + 4HCl \qquad \Delta H = -32 \text{ kcal} \tag{17}$$

Although this reaction has a reasonable negative reaction enthalpy,[33] the ALD surface reactions are very slow and only occur at high temperature after very large $SiCl_4$ and H_2O exposures.[124] The surface reactions for SiO_2 ALD are[74,124−127]

$$\text{(A) } SiOH^* + SiCl_4 \rightarrow SiOSiCl_3^* + HCl \tag{18}$$

$$\text{(B) } SiCl^* + H_2O \rightarrow SiOH^* + HCl \tag{19}$$

Fortunately, SiO_2 ALD can be catalyzed using other molecules. The catalysts for the SiO_2 ALD surface chemistry are Lewis bases such as pyridine or NH_3 (ammonia).[126,127] The SiO_2 ALD growth is catalyzed only when the Lewis base is present during both the $SiCl_4$ and H_2O surface reactions. Additional studies have shown that Lewis bases can also catalyze SiO_2 ALD using other silicon precursors such as $Si(OCH_2CH_3)$ (tetraethoxysilane (TEOS)).[128]

The mechanism for the catalysis is believed to be the hydrogen bonding between the Lewis base and either the SiOH* surface species during the $SiCl_4$ reaction or the H_2O reactant during the H_2O reaction.[126,127,129,130] A schematic illustrating this mechanism is displayed in Figure 13.[127] The hydrogen bonding between the Lewis base and the SiOH* surface species weakens the SiO−H chemical bond and makes the oxygen a stronger nucleophile. This hydrogen bonding interaction facilitates the nucleophilic attack by the oxygen on the electropositive Si atom in the $SiCl_4$ reactant. Likewise, the hydrogen bonding between the Lewis base and the H_2O reactant makes the oxygen in H_2O a stronger nucleophile for nucleophilic attack on the electropositive Si atom in the SiCl* surface species.

The effect of the Lewis base catalyst is very dramatic. Without pyridine as the Lewis base catalyst, SiO_2 ALD using $SiCl_4$ and H_2O as the reactants requires reaction temperatures of >325 °C and reactant exposures of $\sim 10^9$ Langmuirs (1 Langmuir = 1×10^{-6} Torr s).[124] With pyridine as the Lewis base catalyst, SiO_2 ALD can occur at temperatures close to room temperature with reactant exposures of only $\sim 10^4$ Langmuirs.[127] A variety of techniques such as QCM, XRR, ellipsometry, and profilometry have measured very linear SiO_2 ALD at 32 °C in a viscous flow ALD reactor with a growth per cycle of ~1.35 Å.[131] The resulting SiO_2 films have reasonable dielectric properties, although they are inferior to thermal SiO_2 oxide films.

One of the problems with catalytic SiO_2 ALD is the secondary reaction between the pyridine or NH_3 Lewis base catalyst and the HCl reaction product to form a salt.[126,127,129,131] These pyridium or ammonium chloride salts have a finite vapor pressure and will desorb from the growing SiO_2 ALD film. However, the salts can accumulate on the SiO_2 ALD surface and poison the SiO_2 ALD growth if there is insufficient time for desorption. SiO_2 ALD with TEOS as the silicon precursor was attempted to avoid HCl as a reaction product and to eliminate the salt formation.[128] SiO_2 ALD could be accomplished using NH_3 as the catalyst. However, the catalyzed SiO_2 ALD reaction was much less efficient with TEOS compared with $SiCl_4$ as the silicon reactant.[128]

Another limitation of catalytic SiO_2 ALD is the limited temperature range over which the Lewis base can catalyze the SiO_2 ALD surface reactions.[126,127,131] The catalysis requires the presence of the Lewis base on the SiO_2 ALD surface. FTIR investigations can determine the interaction of the pyridine and NH_3 Lewis base catalysts with the SiOH* surface species by monitoring the SiO-H stretching vibration.[129,131] These studies reveal that the Lewis base interaction with SiOH* surface species is progressively removed because of Lewis base desorption at temperatures > 30 °C.[129,131] The desorption temperature can be shifted by the pressure of the Lewis base catalyst. The Lewis base coverage is determined by the steady state established by the Lewis base adsorption and desorption rates.

Other ALD systems should also display similar catalytic effects using Lewis bases. These systems are other metal oxides such as SiO_2, where the MOH* surface hydroxyl is acidic and can transfer a proton to liquid water. The Lewis base will hydrogen bond strongly to these acidic hydroxyl groups and make the oxygen more nucleophilic. Good candidates are metal oxides that are known to have their isoelectric points in water at pH < 7.[132] These metal oxides include TiO_2, ZrO_2, and SnO_2.[132] One study has reported the catalysis of TiO_2 CVD using $TiCl_4$ and H_2O with NH_3 as the Lewis base catalyst.[133]

8. ALD on Polymers

Low temperature ALD enables ALD on thermally sensitive materials such as organic polymers. ALD on polymers may be useful to functionalize the polymer surface, to create unique inorganic/organic polymer composites, and to deposit gas diffusion barriers on polymers. ALD on polymers was not performed until recently because polymers decompose at the temperatures required for many ALD systems. In addition, most polymers do not contain the necessary surface chemical species that were believed to be necessary to initiate ALD.

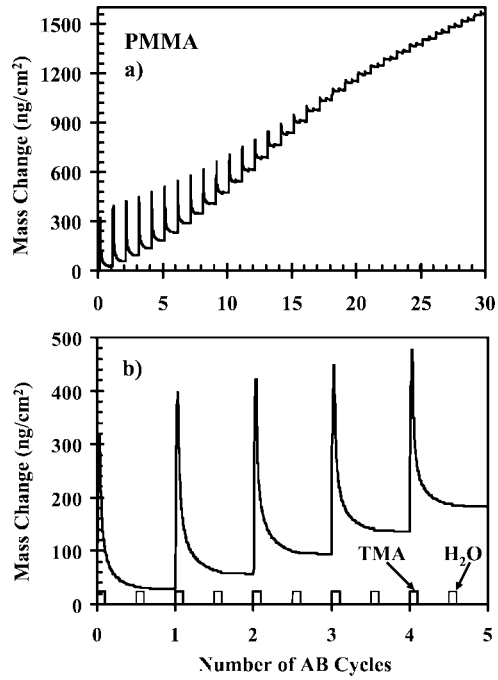

Figure 14. (a) Mass change measured by a quartz crystal microbalance versus the number of AB cycles during Al_2O_3 ALD on PMMA at 85 °C for 30 AB cycles. (b) Mass change at higher mass resolution for the first five AB cycles shown in part a. (Reprinted with permission from ref 134. Copyright 2005 American Chemical Society.)

In situ FTIR studies revealed the nucleation and growth mechanism for Al_2O_3 ALD using $Al(CH_3)_3$ and H_2O as the reactants on polyethylene particles.[36] The H_2O reactant was not observed to interact or adsorb into the polyethylene particles. In contrast, the $Al(CH_3)_3$ reactant was observed to diffuse into the polyethylene. After the adsorption of $Al(CH_3)_3$, the subsequent H_2O exposure led to the reaction of H_2O with $Al(CH_3)_3$ to form AlOH* species. These AlOH* species are believed to be from $Al(OH)_4$ clusters in the near surface region of the polyethylene particles. The FTIR studies also observed the progressive growth of infrared features consistent with bulk Al_2O_3.[36] Subsequent examination after 40 ALD cycles revealed the presence of a thin Al_2O_3 film on the polyethylene particles.

Additional QCM studies of Al_2O_3 ALD on polymer films spin-coated onto QCM sensors further clarified and confirmed the mechanism for ALD on polymers.[134] The QCM investigations observed the nucleation and growth of Al_2O_3 ALD on polymer films with thicknesses from 2400 to 4000 Å. A variety of polymers were studied, including polymethylmethacrylate (PMMA), polypropylene, polystyrene, polyethylene, and polyvinylchloride. The key observation from the QCM studies was the large mass gain and loss corresponding to the diffusion of $Al(CH_3)_3$ into the polymer film during TMA exposure and out of the polymer film after the TMA exposure during the initial ALD cycles.

The diffusion effects were especially pronounced on the PMMA polymer films. QCM results for Al_2O_3 ALD for the first several ALD cycles on PMMA at 86 °C are shown in Figure 14.[134] Figure 14a shows the QCM results during the first 30 Al_2O_3 AB cycles. Figure 14b displays the QCM results for the first 5 Al_2O_3 AB cycles. These results show that the diffusion of TMA in and out of the PMMA polymer film was only observed for the first 10−15 ALD cycles.[134] As the Al_2O_3 ALD film grows in the near surface region of

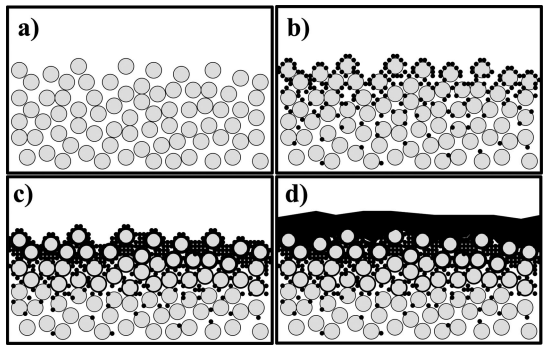

Figure 15. Model for Al_2O_3 ALD on polymer films showing (a) a cross section of the polymer chains at the surface of the polymer film, (b) Al_2O_3 nucleation clusters formed from H_2O reaction with TMA trapped in the near surface region, (c) coalescence of Al_2O_3 clusters and closure of the space between the polymer chains, and (d) formation of a dense Al_2O_3 film that grows on top of the polymer surface. (Reprinted with permission from ref 134. Copyright 2005 American Chemical Society.)

the polymer and begins to form a continuous film, the Al_2O_3 ALD film hinders the TMA diffusion. This Al_2O_3 barrier film then prevents any TMA diffusion and the QCM measurements observe only the linear growth of the Al_2O_3 ALD film after >15 ALD cycles.

These results suggest the following mechanism for ALD on polymers:[134] (1) one of the ALD precursors, such as TMA, diffuses into the near surface region of the polymer; (2) clusters of the ALD material form in the near surface region as a result of the bimolecular reaction between the two ALD precursors; (3) the clusters grow and eventually begin to coalesce; (4) a continuous film is formed that prevents the diffusion of additional precursor into the polymer; and (5) the ALD material grows linearly on the continuous ALD film. This mechanism is illustrated in Figure 15.[134] The open circles represent a cross section of polymer chains.

The QCM results suggest that the Al_2O_3 ALD films using $Al(CH_3)_3$ and H_2O may be effective gas diffusion barriers on polymers. Additional studies have explored the use of Al_2O_3 ALD films as gas diffusion barriers. Investigations of Al_2O_3 ALD on polyethylenenaphthalate (PEN) and Kapton have shown that Al_2O_3 ALD films as thin as 10 nm can reduce the water vapor transmission rate (WVTR) over 3 orders of magnitude to $\leq 1 \times 10^{-3} - 1 \times 10^{-4}$ g/m^2/day depending on the test measurement technique.[135,136] Even lower WVTRs were measured with bilayer or multilayer barriers fabricated using Al_2O_3 ALD and SiN plasma-enhanced CVD,[137] Al_2O_3 ALD and rapid SiO_2 ALD,[138] and Al_2O_3 ALD and ZrO_2 ALD.[139] Other studies using plasma ALD with $Al(CH_3)_3$ and O_2 plasma have also produced very effective Al_2O_3 ALD gas diffusion barriers with WVTR $\sim 5 \times 10^{-3}$ g/m^2/day.[61]

Many of the applications for ALD on polymers have utilized Al_2O_3 ALD. Al_2O_3 ALD has been employed to encapsulate organic light emitting diodes[140,141] and organic solar cells[142] for hermetic sealing to prevent H_2O permeation. Al_2O_3 ALD has also been effective as a capping layer[143] and a gate dielectric[144] for polymer-based transistors. Surface modification of natural fiber and woven fabric materials has utilized Al_2O_3 ALD.[145] Al_2O_3 ALD on electrospun polymer fibers has also been used to fabricate Al_2O_3 microtubes.[146] Polymers have also been protected from erosion by oxygen atoms using Al_2O_3 ALD.[147] In addition to Al_2O_3 ALD, TiO_2 ALD on polystyrene spheres has been employed to fabricate nanobowl arrays,[148] TiO_2 ALD and ZrO_2 ALD on polycarbonate membranes has been utilized to form TiO_2 and ZrO_2 nanotubes,[149] and W ALD has been demonstrated to form tungsten metal films on polymers.[150]

9. ALD on High Aspect Ratio Structures

The ability of ALD to deposit on high aspect ratio structures is one of the most desirable characteristics of ALD. The miniaturization of semiconductor devices has led to the increasing need for ALD to coat high aspect ratio structures. The main examples are the deposition of Cu diffusion barriers for backend interconnects[51] and the deposition of dielectric layers to fabricate DRAM capacitors for memory storage.[2] Outside of the semiconductor industry, the ability of ALD to deposit on high aspect ratio structures is also useful for ALD fabrication of the half-gap dielectric on magnetic read/write heads[3] and ALD on MEMS devices for surface functionization and protection.[151]

ALD on high aspect ratio structures can be understood by model studies of ALD on well-defined structures with high aspect ratios. One such well-defined structure is anodic aluminum oxide (AAO).[152] AAO is defined by linear pores that are aligned approximately parallel to each other. In addition, the pores are arranged with approximately hexagonal symmetry. The preparation of AAO is achieved by electrochemical anodization of aluminum films. This anodization yields AAO films with typical thicknesses of $\sim$50 μm and pore diameters of $\sim$50 nm for an aspect ratio of $\sim$1000.

Studies of Al_2O_3 ALD in AAO using scanning electron microscopy (SEM) analysis have revealed that conformal ALD coating of high aspect ratio structures is dependent on the ALD exposure times.[153] For AAO with a thickness of $\sim$50 μm and pore diameters of $\sim$65 nm that were open to the gas phase ALD reactants on both sides of the AAO film, exposure times of 1 s were insufficient to obtain a conformal ALD coating in the interior of the AAO film. Reactant exposures of $\sim$30 s were required to obtain a nearly conformal coating.[153]

Additional investigations of ZnO ALD on AAO were performed using electron microprobe analysis with energy dispersive spectroscopy (EDS).[153] These EDS studies were able to resolve the ZnO coverage on the AAO pores versus distance into the AAO film. ZnO coverages were observed that decreased versus distance into the AAO film, as shown in Figure 16a.[153] The decrease was much sharper for the shorter ALD exposure times. The ZnO ALD coverage could be integrated to obtain the total amount of ZnO ALD in the AAO film versus exposure time, as displayed in Figure 16b.[153] The integrated ZnO ALD coverage increased with $t^{1/2}$, where t is the exposure time. These results are consistent with gas diffusion limiting the flux of reactants into the pores of AAO.

The $t^{1/2}$ dependence of the integrated ZnO ALD coverage versus exposure time suggested that the ZnO ALD could be understood using kinetic gas theory. Consequently, Monte Carlo modeling was performed assuming that the ZnO ALD was limited by the diffusion of diethylzinc in the pores of AAO.[153] This modeling confirmed the $t^{1/2}$ dependence and obtained nearly quantitative agreement with the integrated ZnO ALD coverage using the known parameters for the system with no fitting parameters. This agreement suggests that ALD in high aspect ratio structures can be understood in terms of gas kinetic theory with ALD reactants in molecular flow.

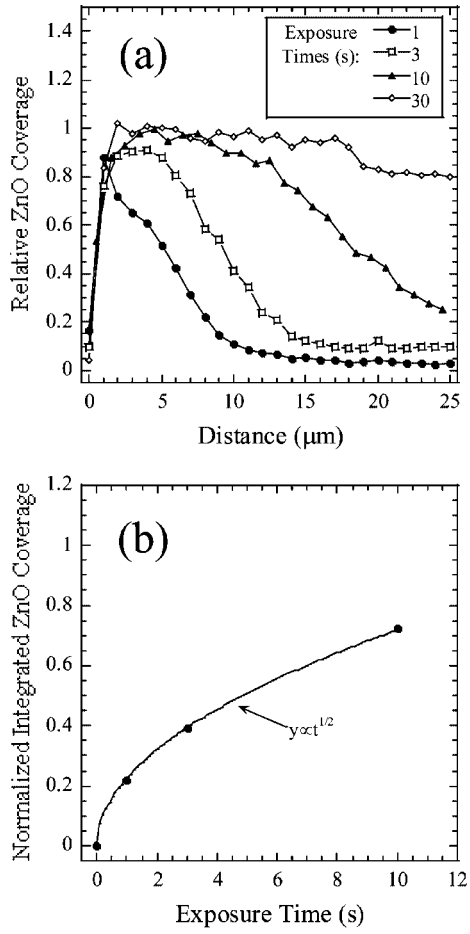

Figure 16. (a) Relative ZnO coverage measured by electron probe microanalysis line scan and (b) normalized integrated ZnO coverage following 64 AB cycles of ZnO ALD using exposure times of 1, 3, 10, and 30 s. (Reprinted with permission from ref 153. Copyright 2003 American Chemical Society.)

The exposure time required to obtain conformal ALD in high aspect ratio structures can be predicted using the results from the Monte Carlo modeling. The results from the simulations for ZnO ALD in high aspect ratio cylinders yield the relationship $T = 1/k^2$, where T is the exposure time required for the normalized integrated coverage, Θ^*, to reach $\Theta^* = 1$. The parameter k is given by[153]

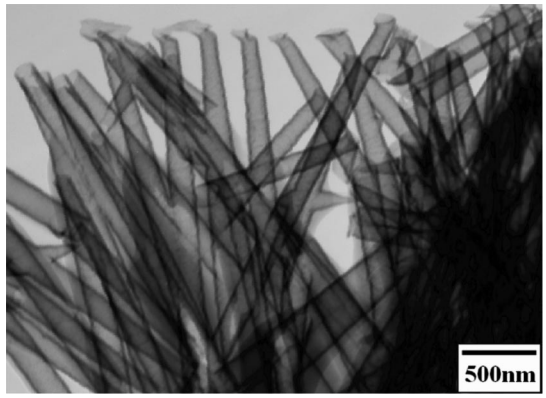

Figure 17. TEM image of ZrO_2 nanotubes fabricated in polycarbonate templates with 200 nm pores. The ZrO_2 nanotubes are 200 nm in diameter. (Reprinted with permission from ref 149. Copyright 2004 John Wiley & Sons.)

$$k\ (s^{-1/2}) = 2.1 \times 10^3\ P^{1/2} m^{-1/4} N^{-1/2} (d/L) \quad (20)$$

In this equation, P is the pressure (Torr), m is the mass (amu) of diethylzinc for ZnO ALD, N (cm^{-2}) is the number of surface sites, and the aspect ratio is L/d, where L and d are the length and diameter of the cylinder.

The relationship $T = 1/k^2$ indicates that the required exposure time for conformal ALD scales as the square of the aspect ratio, i.e. $T \propto (L/d)^2$. As an example of using this relationship, for $P = 5$ Torr, an aspect ratio of $L/d = 5000$, $m = 123$ amu for diethylzinc, and $N = 0.84 \times 10^{15}$ cm^{-2}, the required exposure time for conformal ALD is $T = 11$ s. Although longer times are required for high aspect ratios, the required exposure times are not prohibitively long even for high aspect ratios.

Another treatment has derived the required exposure times for conformal ALD using gas conductance equations.[154] This treatment also predicts that the required exposure for conformal ALD scales as the square of the aspect ratio in the limit of large aspect ratios. Assuming a unity reactive sticking coefficient, the total required exposure is equal to the product of the pressure, P, and the time, t, and is given by[154]

$$(Pt)_{\text{total}} = S(2\pi mkT)^{1/2}\{1 + ({}^{19}/_{4})(L/d) + ({}^{3}/_{2})(L/d)^2\} \quad (21)$$

In this equation, S is the saturated surface density and L/d is the aspect ratio for a cylinder.

$S(2\pi mkT)^{1/2}$ is the exposure required for a flat surface to be reacted to completion assuming a unity reactive sticking coefficient.[154] A reactive sticking coefficient, Γ, less than unity will increase the exposure according to $S(2\pi mkT)^{1/2}/\Gamma$. In the limit of large aspect ratios, the $(L/d)^2$ term dominates in the term $\{1 + (19/4)(L/d) + ({}^{3}/_{2})(L/d)^2\}$ and the required exposure is proportional to the square of the aspect ratio. The exposure time derived from eq 21 can be shown to agree with the exposure time $T = 1/k^2$, where k is given by eq 20.

There are many examples of ALD on high aspect ratio structures. Outside of the semiconductor arena, ALD on high aspect ratio MEMS devices is important to deposit protective coatings,[151,155] hydrophobic layers,[156] and lubricating films.[157] As mentioned earlier when discussing ALD on polymers, ALD on porous polycarbonate membranes is utilized for nanotube fabrication[149] and ALD on self-assembled polystyrene spheres allows for the formation of nanobowl arrays.[148] Figure 17 shows a TEM image of ZrO_2 ALD nanotubes fabricated in a high aspect ratio polycarbonate membrane with 200 nm pore diameters.[149]

ALD on AAO has been utilized to form Fe_2O_3 nanotube arrays with controlled geometry and tunable magnetism.[158] Ferromagnetic Ni and Co nanotubes have also been grown in AAO using ALD methods.[159] ALD on high aspect ratio self-assembled opal structures has been employed for the fabrication of photonic crystals.[123,160−162] ALD on porous substrates and aerogels has also been a novel avenue for the fabrication of high surface area catalysts.[163−165]

10. ALD on Particles

There are many applications for ALD on particles. The surface chemical properties of particles can be modified by ALD while retaining the bulk properties of the original particles. ALD can also deposit protective and insulating coatings on particles to prevent particle oxidation[166] or

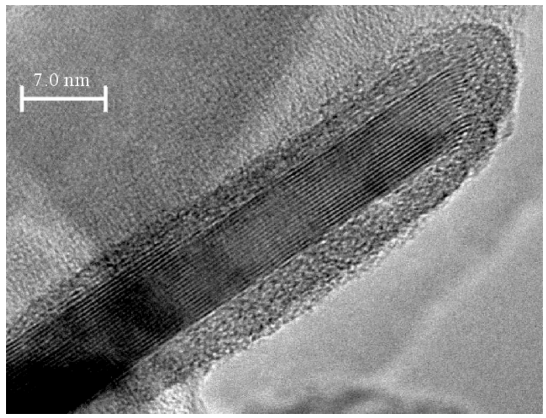

Figure 18. TEM image of HCV grade BN coated with Al_2O_3 ALD in a fluidized bed reactor. (Reprinted with permission from ref 172. Copyright 2004 Elsevier.)

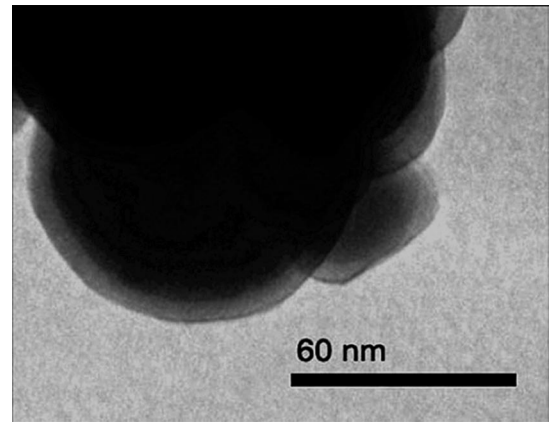

Figure 19. TEM image of ZrO_2 nanoparticles with an average diameter of 62 nm coated with 50 AB cycles of Al_2O_3 ALD. (Reprinted with permission from ref 41. Copyright 2007 American Institute of Physics.)

electrical conduction.[167] ALD coatings on particles can also serve to modify the optical[168] or mechanical[169] properties of the particles. In addition, various composite core/shell structures can be fabricated using ALD on particles that may have a designed chemical reactivity.[170]

ALD on particles depends on the ability of ALD to produce conformal coatings on high aspect ratio structures. A bed of particles will have an effective aspect ratio that is defined by the particle size and shape.[41] A static particle bed will appear to the gas phase ALD reactants like a porous substrate.[41] A bed of fluidized particles will have much higher gas conductance.[171] The moving particles will allow the gas phase ALD reactants to encounter all the accessible particle surface area in a much shorter time. The agitation of the particles will also prevent the individual particles from being "glued together" in the particle bed by the ALD coating.

ALD on particles has been demonstrated in a fluidized particle bed.[172,173] During fluidization, the upward force of the pressure drop across the particle bed equals the downward force of gravity on the particle bed. The equal forces lead to the fluidation of the particles. Although particle aggregates form during fluidization, the aggregates are dynamic and the constant exchange of particles between the aggregates prevents the particles from being "glued together" during ALD. The initial demonstration of ALD on particles in a fluidized bed performed Al_2O_3 ALD on BN particles.[172] Excellent conformal coatings of Al_2O_3 ALD were observed on BN particles with a platelet shape as shown by the TEM image in Figure 18.[172]

ALD on particles has also been demonstrated in a rotary reactor that tumbles the particles in a porous metal cylinder to prevent agglomeration.[41] In contrast to the fluidized bed reactor, the rotary reactor can be operated using static exposures because a constant gas flux is not needed to fluidize the particles. The static exposures allow for much higher precursor utilization for efficient ALD surface reactions. High precursor utilization is especially critical for high surface area nanoparticles. Al_2O_3 ALD on ZrO_2 nanoparticles has been characterized in the rotary reactor.[41,174] A TEM image of a ZrO_2 nanoparticle coated in the rotary reactor with 80 AB cycles of Al_2O_3 ALD is shown in Figure 19.[41]

ALD on nanostructures such as nanotubes and nanowires faces similar issues to ALD on particles. For large quantities of nanotubes or nanowires, the nanostructures will also need to be fluidized or agitated in a rotary reactor to obtain high gas conductance for efficient ALD reactions. For many of the reported studies of ALD on nanotubes and nanowires, the ALD was performed on individual nanostructures that provided adequate gas conduction without needing fluidization or agitation. Some of the early examples for ALD on nanotubes and nanowires include Al_2O_3 ALD on multiwalled carbon nanotubes (CNTs)[175] and Al_2O_3 ALD on ZnO nanorods.[176] Coaxial $Al_2O_3/W/Al_2O_3$ multilayer coatings were also demonstrated on multiwalled CNTs.[177] As mentioned earlier in section 6, Al_2O_3 ALD has also been demonstrated on single-walled CNTs.[116,117]

11. ALD of Nanolaminates and Alloys

The ALD of nanolaminates and alloys has many applications in semiconductor device fabrication and nanostructure engineering. The first report of nanolaminates fabricated using ALD examined HfO_2/Ta_2O_5 nanolaminates as low leakage dielectric films.[178] The HfO_2/Ta_2O_5 nanolaminates could be tuned to improve the charge storage in dielectric films. Other studies have demonstrated extremely conformal deposition of Al_2O_3/Ta_2O_5 and $Hf_xAl_yO_z$ alloy stacks in trench capacitors for DRAM capacitors.[2] Al_2O_3/TiO_2 nanolaminates with layer thicknesses much smaller than the wavelength of light have also been employed to tune the optical refractive index of the nanolaminate film over a wide range from $n = 2.4$ for TiO_2 to $n = 1.6$ for Al_2O_3.[179]

Nanolaminates can also be fabricated that display novel physical properties because the layer thickness is less than or equal to the length scale that defines the physical property.[180] For example, extremely hard films can be constructed when the layer thickness is less than the slip plane dislocation length. Thermal barrier coatings can be fabricated when the layer thickness is less than the phonon mean free path in the material. Studies of thermal conductivity have revealed that the thermal conductivity in Al_2O_3/W nanolaminates can decrease below the minimum value for yttria-stabilized ZrO_2.[181] The Al_2O_3/W nanolaminate was effective as a thermal barrier coating because of the large frequency difference between phonons in Al_2O_3 and W.[182]

Other studies have explored the use of TiO_2/Al_2O_3,[183] AlP/GaP,[184] and Al_2O_3/W[6] nanolaminates as Bragg mirrors. The 16-bilayer Al_2O_3/W superlattice displayed a reflectivity of ~96% in the hard X-ray region for the Cu Kα line at $\lambda = 1.52$ Å.[6] This reflectivity is the highest reflectivity reported for a first-order Bragg peak in the hard X-ray region. In addition, Bragg peaks from this nanolaminate were observed

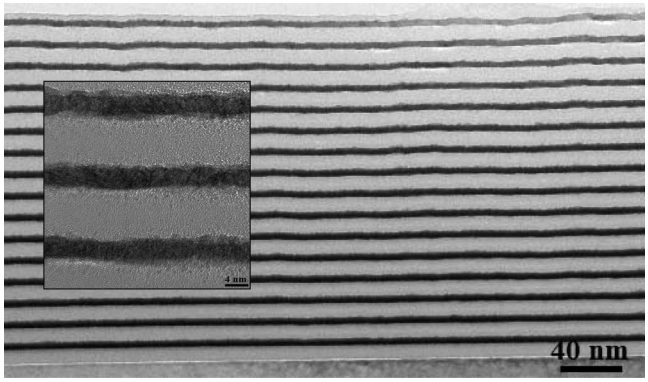

Figure 20. TEM image of a 16-bilayer Al_2O_3/W superlattice optimized for X-ray reflectivity at $\lambda = 1.54$ Å. The inset shows a high resolution TEM image. (Reprinted with permission from ref 6. Copyright 2006 American Institute of Physics.)

at larger angles up to the sixth-order Bragg peak. A TEM of this 16-bilayer Al_2O_3/W superlattice is shown in Figure 20.[6] Additional studies demonstrated high X-ray reflectivity for six-bilayer Al_2O_3/W superlattices deposited on polyethylenenaphthalate (PEN) substrates.[185] The resulting X-ray mirrors were extremely flexible and could be adjusted to obtain a wide range of curvatures.

The precise control over individual surface reactions during ALD also allows for the fabrication of alloys and graded materials. For example, if the temperature for the ALD reactions is similar for two ALD systems forming an alloy, then the alloy can be grown by alternating back-and-forth between the ALD cycles for the first material and the ALD cycles for the second material. The composition of the alloy can be controlled by the relative number of ALD cycles for each material. The relative number of ALD cycles of each material could also change progressively to fabricate a graded material.

An example of an alloy grown using ALD is the Al_2O_3/ZnO alloy. The Al_2O_3/ZnO alloy can be grown by alternating between the TMA and H_2O reaction cycles for Al_2O_3 ALD and the diethylzinc and H_2O reaction cycles for ZnO ALD.[186]

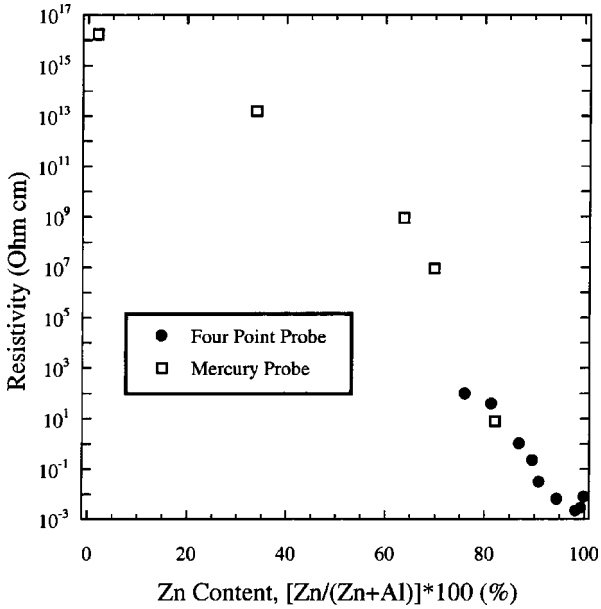

Figure 21. Resistivity of ZnO/Al_2O_3 alloy films measured using a four-point probe and a mercury probe. (Reprinted with permission from ref 187. Copyright 2003 The Electrochemical Society.)

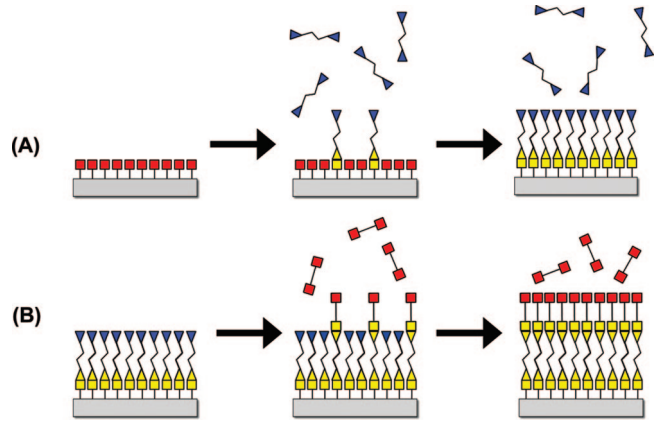

Figure 22. Schematic representation of MLD using self-limiting surface chemistry and an AB binary reaction sequence. (Reprinted with permission from ref 190. Copyright 2007 American Chemical Society.)

Although there are nucleation issues upon initiating the Al_2O_3 ALD cycles following the ZnO ALD cycles,[186] the relative number of Al_2O_3 ALD and ZnO ALD cycles can be changed to define a wide range of alloy compositions. Since Al_2O_3 ALD films are insulating and ZnO ALD films are conducting, variable resistivity films can be fabricated using Al_2O_3/ZnO alloys.[187] The resistivity of these alloys varies continuously from $\sim 10^{16}$ Ω cm for pure Al_2O_3 ALD to $\sim 10^{-2}$ Ω cm for pure ZnO ALD, as shown in Figure 21.[187] These alloys have been employed to define charge dissipative coatings for RF MEMS switches.[188]

12. Polymer MLD

12.1. Organic Polymers

ALD processes have been developed for a wide range of inorganic materials. Similar self-limiting surface reactions can be employed for the growth of organic polymers. This film growth is described as molecular layer deposition (MLD) because a molecular fragment is deposited during each ALD cycle.[189] A cartoon illustrating the MLD process is shown in Figure 22.[190] MLD was initially developed for the growth of organic polymers such as polyamides[191] and polyimides.[189] The self-limiting surface strategies for MLD have also been called alternating vapor deposition polymerization (AVDP).[191] MLD developed from an earlier gas-phase polymer growth method known as vapor deposition polymerization (VDP).[192]

More recent work has renewed interest in the MLD of organic polymers.[193] The MLD of various polyamides using acyl chlorides and amines as the reactants has been studied using in situ Fourier transform infrared (FTIR) spectroscopy.[190,194] For poly(*p*-phenylene terephthalamide) (PPTA) MLD, the acyl chloride is terephthaloyl chloride ($ClCOC_6H_4COCl$) (TC) and the diamine is *p*-phenylenediamine ($NH_2C_6H_4NH_2$) (PD). The surface reactions for PPTA MLD are proposed as follows:[194]

$$(A)\ -NH_2^* + ClCOC_6H_4COCl \rightarrow -NHCOC_6H_4COCl^* + HCl \quad (22)$$

$$\text{(B)} \; -\text{NHCO}(\text{CH}_2)_4\text{COCl}^* + \text{H}_2\text{NC}_6\text{H}_4\text{NH}_2 \rightarrow -\text{NHCOC}_6\text{H}_4\text{CONH}(\text{CH}_2)_6\text{NH}_2^* + \text{HCl} \quad (23)$$

where the asterisks again designate the surface species. The FTIR measurements observe self-limiting reactions during TC and PD exposures. The PPTA MLD growth is linear but varied between 0.5 and 4.0 Å per AB cycle for individual experiments. This variability was attributed to varying numbers of "double" reactions between the bifunctional reactants and the surface species.[194]

A number of other organic polymers have also been grown using MLD techniques. The MLD of polyurea using 1,4-phenylene diisocyanate and ethylene diamine as the reactants has been investigated using total internal reflection FTIR techniques.[195] Additional studies have also demonstrated the temperature-dependent MLD growth of polyimides using pyromellitic dianhydride (PMDA) and various diamines[196] and the MLD of polyurethane using 1,4-phenylene diisocyanate and 2-butyne-1,4-diol.[197] Other recent investigations have demonstrated the area-selective patterning[198] and orientation control[199] of polyazomethine MLD. Polyazomethine is a conjugated polymer grown using terephthalaldehyde and *p*-phenylenediamine as the MLD reactants.[199,200]

12.2. Hybrid Organic−Inorganic Polymers

In addition to organic polymers, the MLD of hybrid organic−inorganic polymers has been demonstrated using inorganic precursors from ALD with various organic precursors.[193] One class of hybrid organic−inorganic MLD polymer is the "alucones".[201] These hybrid polymers result from using aluminum alkyl precursors such as trimethylaluminum (TMA) and various organic diols such as ethylene glycol (EG).[201] The surface reactions during alucone MLD can be written as[201]

$$\text{(A)} \; \text{MR}^* + \text{HOR'OH} \rightarrow \text{MOR'OH}^* + \text{RH} \quad (24)$$

$$\text{(B)} \; \text{R'OH}^* + \text{MR}_x \rightarrow \text{R'OMR}_{x-1}^* + \text{RH} \quad (25)$$

where the metal alkyl molecule is MR_x and the diol is HOR′OH. A schematic illustrating the MLD of alucone using TMA and EG is shown in Figure 23.[201]

The MLD of alucones is very robust and yields very efficient and linear growth. Alucone MLD using TMA and EG has been investigated using a quartz crystal microbalance (QCM) and in situ FTIR investigations.[201] The growth rate per cycle was observed to decrease from 4.0 Å per AB cycle at 85 °C to 0.4 Å per AB cycle at 175 °C.[201] In addition to alucone MLD, other studies have explored the growth of hybrid zinc/organic polymers that can be referred to as "zincones".[202,203] Zincone MLD is also very efficient and leads to linear growth.[202,203] A wide range of various hybrid organic−inorganic polymers are possible, as described by a recent patent application.[204]

There are a number of difficulties for MLD relative to ALD.[193] MLD usually has problems with the low vapor pressure of the organic precursors. In addition, organic precursors are also thermally sensitive and will decompose at higher temperatures. The low vapor pressure of the organic precursors cannot always be solved by raising the temperature of the precursor source. The resulting MLD polymer films are also fairly porous. Consequently, the ALD and MLD reactants can diffuse into the MLD films. This precursor diffusion leads to an additional growth mechanism for MLD films. The MLD films can grow either by self-limiting surface reactions or by a type of CVD reaction between reactants that have diffused into the MLD film. Despite these difficulties, MLD film growth has displayed self-limiting and linear growth that is very similar to ALD.

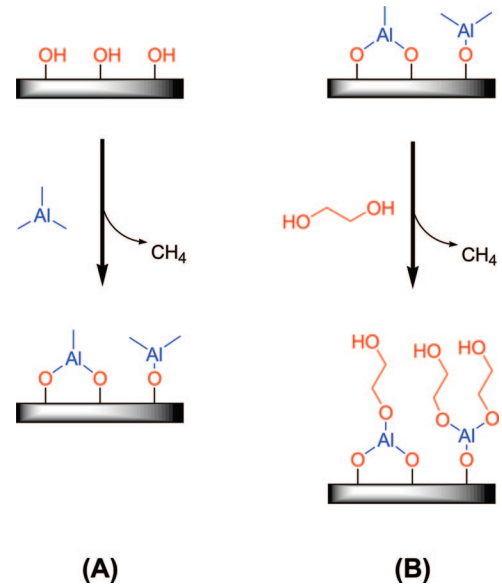

Figure 23. Illustration of surface chemistry for two-step alucone MLD using TMA and EG as reactants. (Reprinted with permission from ref 201. Copyright 2008 American Chemical Society.)

Another difficulty during MLD is that the homobifunctional organic precursors typically employed during MLD can react more than once with the chemical groups on the surface.[193,194] These "double" reactions lead to a loss of active surface sites and the reduction of the MLD growth per cycle. To avoid these "double" reactions with homobifunctional

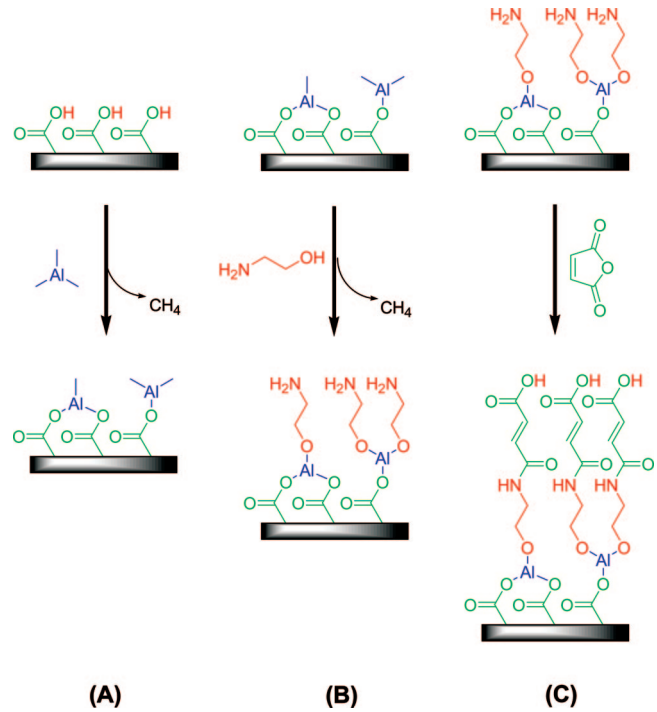

Figure 24. Illustration of surface chemistry for three-step alucone MLD with TMA, EA, and MA as reactants. (Reprinted with permission from ref 193. Copyright 2009 American Chemical Society.)

organic precursors, alternative organic precursors can be employed such as heterobifunctional organic precursors and ring-opening reactions.[193,194] This new strategy is developing and has been demonstrated by the MLD of the ABC alucones using three sequential surface reactions with TMA, ethanolamine (EA), and maleic anhydride (MA) as the reactants, as displayed in Figure 24.[193] Many other combinations of reactants are possible, and the MLD of polymer films is expected to develop rapidly in the coming years.

13. Additional Topics

There are various other topics that could have been included in this overview of ALD. The field of ALD is growing rapidly and expanding into many applications outside of semiconductor processing. This overview has attempted to capture many of the main themes and applications of ALD. Everything could not be included because of space and the need to establish priorities. However, there are several additional topics that should be mentioned which are given below.

13.1. Nonideal ALD Behavior and the ALD Window

The ideal model for ALD displayed by Al_2O_3 ALD may not be achieved by other ALD systems. Some ALD systems are not self-limiting because the surface species may decompose and allow additional adsorption. This decomposition may occur even at the minimum temperatures required for the surface reactions. Other ALD systems may be based on surface reactions that never reach completion. These reactions may proceed to some percentage of completion and then stop. These reactions will display self-limiting growth but with large amounts of impurities remaining in the films.

The processing temperature range for ALD or the so-called "ALD window" is the region of nearly ideal ALD behavior between the nonideal regions as shown in Figure 25.[12] At lower temperatures, the reactants could condense on the surface or the surface reactions may not have enough thermal energy to reach completion. At higher temperature, the surface species could decompose and allow additional reactant adsorption. This behavior is similar to CVD by unimolecular decomposition. The surface species needed for ALD could also desorb from the surface at higher temperatures and be unavailable for additional surface reactions. This desorption would lead to the decrease of the ALD growth per cycle at higher temperatures. This behavior is observed for Al_2O_3 ALD.[14,20,32]

One system that displays dramatic nonideal ALD behavior is TiN ALD using tetradimethylaminotitanium (TDMAT) and NH_3. Although this ALD system was initially presented as a working ALD process,[205,206] additional studies revealed that the surface reactions did not reach completion, impurities were left in the resulting films, and the films had significant porosity that led to their easy oxidation.[64] TiN ALD using TDMAT and NH_3 has no "ALD window" where the ALD process is reasonable. In contrast, TiN ALD using $TiCl_4$ and NH_3 is a well-defined ALD process that occurs at higher temperatures and produces HCl as a reaction product.[207]

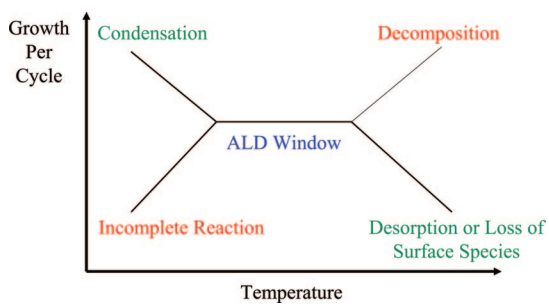

Figure 25. Schematic of possible behavior for the ALD growth per cycle versus temperature showing the "ALD" window. (Adapted from ref 12.)

13.2. Area-Selective ALD for Spatial Patterning

ALD has exquisite control over the thickness of the deposited thin film. However, lateral patterning of ALD is needed for fabrication of three-dimensional devices. Lateral patterning can be achieved using photoresist and photolithography methods that are similar to conventional semiconductor processing. Self-assembled monolayers can also be used as a masking layer. In addition, direct write methods such as electron beam writing can be used to remove the masking layer and allow for ALD on the selected surface areas.

One example of area-selective ALD is the lateral patterning of HfO_2 ALD on Si(100).[208,209] Area-selective blocking chemistry was observed using siloxane attachment to SiO_2 surfaces. In this demonstration, photolithography was initially used to produce a patterned SiO_2 surface on Si(100). The areas not covered with SiO_2 remained as the hydrogen-passivated H−Si(100) surface. Subsequently, the surface was exposed to octadecyltrichlorosilane (ODTS) and a self-assembled siloxane monolayer formed on the SiO_2 surface. The HfO_2 ALD was then performed and the HfO_2 ALD layer grew only on the H−Si(100) areas of the surface. Scanning Auger analysis revealed the laterally patterned HfO_2 ALD surface.[209]

Area-selective ALD has also been demonstrated for other ALD systems. Lateral patterning of Ru ALD has been achieved using patterned octadecyltrichorosilane monolayers.[210] Spatial selectivity has also been demonstrated for Pt ALD using a monolayer resist of 1-octadecene adsorbed to the hydride-terminated silicon regions of a Si/SiO_2 substrate.[211] In addition, the selective deposition of TiO_2 ALD has been reported using polymer masking layers.[212−214] HfO_2 ALD has also been patterned using the pores of S-layer proteins as a template.[215] As mentioned earlier, area-selective Cu ALD was demonstrated on platinum seeded substrates.[95] The lateral patterning of a polyazomethine MLD film was also achieved by selective MLD on the hydrophilic regions of a hydrophobic/hydrophilic surface.[198]

13.3. Atmospheric Pressure ALD

The cost of ALD is largely tied to the cost of the reactants and the equipment. Most ALD is performed with vacuum pumps that act to move the reactants and products through the reactor and maintain a clean environment in the reactor. These vacuum pumps are not needed if ALD could be performed at pressures greater than atmospheric pressure where the reactant and product gases could be pushed through the reactor. Except for the greater gas usage and the lower gas diffusion rates at higher pressure, atmospheric pressure ALD should be viable and has been demonstrated for ZrO_2 ALD using $ZrCl_4$ and O_2[216] and for HfO_2 ALD using $HfCl_4$ and O_2.[217]

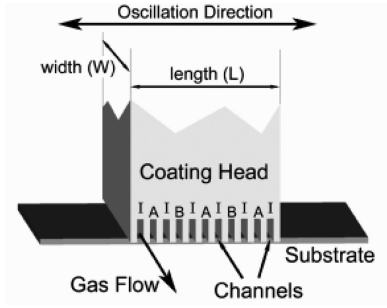

Figure 26. Schematic of an ALD coating head showing the gas channels and gas flow. A is the oxidizing reactant, B is the metal reactant, and I is the inert gas. (Reprinted with permission from ref 218. Copyright 2008 American Institute of Physics.)

A recent design for spatially selective atmospheric ALD has been presented based on a coating head that is positioned next to a substrate.[218] The ALD reactants are delivered through channels in the coating head.[218] The channels are separated by inert gas flow to prevent the gas phase reactions of the precursors. The arrangement of neighboring channels is I/A/I/B..., where I is the inert gas and A and B are the ALD reactants. A schematic illustrating this arrangement of neighboring channels in the coating head over a substrate is shown in Figure 26.[218] Additional pumping channels could also be inserted between the neighboring channels to remove the gases from the region between the coating head and the substrate.

If the coating head is stationary on the substrate, then there is no ALD because each area of the substrate under the coating head is only exposed to one of the two ALD reactants. If the coating head moves relative to the substrate, then the substrate will experience exposure to both ALD reactants. The coating head could either move in a linear fashion or move back and forth to overlap the adjacent surface areas and achieve ALD. This design has been demonstrated for Al_2O_3 ALD and ZnO ALD.[218] Similar saturation behavior was observed for Al_2O_3 ALD compared with conventional Al_2O_3 ALD. The Al_2O_3 ALD films also had excellent insulating properties and have been used to fabricate ZnO thin film transistors.[219]

13.4. ALD on Biological Templates

The complexity of biological structures can be replicated by coating ALD films on biological templates. Low temperature ALD facilitates using the nanostructures of nature as a mold.[24] One of the first demonstrations of ALD on biological templates was TiO_2 ALD and Al_2O_3 ALD on the tobacco mosaic virus (TMV) and ferritin.[122] TiO_2 ALD on the TMV formed extremely small porous structures that replicated the outer protein sheath of the virus. The virus was then decomposed at higher temperatures or removed by a chemical reaction to yield very small nanotubes.[122] Al_2O_3 ALD and TiO_2 ALD on ferritin also demonstrated that ALD can decorate assemblies of biological macromolecules.[122]

Al_2O_3 ALD has also been employed to replicate butterfly wings.[220] SEM images and optical reflectivities revealed that the Al_2O_3 ALD coating was a nearly perfect duplicate of the butterfly wing. This biological duplicate served as a photonic bandgap structure. Additional studies have explored the optical properties of these biological replicas versus TiO_2 ALD thickness.[221] The TiO_2 ALD films acted as Fabry−Perot etalons with reflectivity that was precisely controlled by the TiO_2 ALD film thickness.

13.5. Other Emerging Areas

The main virtues of ALD are its precise thickness control and its extreme conformality on high aspect ratio structures. These virtues have been recognized by additional emerging application areas. A recent review has highlighted the applications of ALD to nanofabrication and emerging nanodevices.[23] One example is ALD for the deposition of conformal coatings with precise thicknesses to form nanowire FETs.[222] ALD may also be useful in fabricating high sensitivity sensors. These sensors can be based on high surface area substrates that are coated with the appropriate sensing film deposited using ALD.[26,223]

ALD may also be useful in the fabrication of nanophotovoltaic (nano-PV) light-harvesting devices. These nano-PV devices are dependent on the close proximity of electron and hole collecting materials. ALD can infiltrate various semiconducting and conducting materials to fabricate efficient structures.[224,225] In addition, biological implants usually require coatings to ensure that they are biocompatible. Some of these implants have high aspect ratios such as coronary artery stents. Various ALD materials such as Al_2O_3 ALD have been explored as biocompatible coatings.[226]

14. Conclusions

Because of continued device miniaturization, control of thin film growth is needed at the atomic level to fabricate semiconductor and other nanoscale devices. To meet these demands, atomic layer deposition (ALD) techniques have been developed for the growth of ultrathin and conformal films. ALD is a gas phase method based on sequential, self-limiting surface reactions. ALD can deposit very conformal and ultrathin films on substrates with very high aspect ratios. This overview has presented a brief introduction to ALD and its history. Subsequently, Al_2O_3 ALD was introduced as a model ALD system. The overview then described other examples of thermal ALD and radical-enhanced ALD for the deposition of single-element metals and semiconductors. Following a brief review of ALD reactor design, the thermal chemistry for metal ALD was also reviewed using fluorosilane elimination chemistry with metal fluorides, combustion chemistry with organometallic precursors, or hydrogen reduction chemistry.

The overview then considered the topic of nucleation and growth during ALD that is extremely important for the ALD of high-*k* gate oxides on H−Si(100). Many topics were then reviewed, including low temperature ALD using Al_2O_3 ALD or catalytic SiO_2 ALD. The overview considered ALD on polymers and the mechanism for ALD on polymers. Molecular layer deposition (MLD) of polymers was also discussed as an analogous process to ALD that can deposit organic and hybrid organic−inorganic polymers. The overview then considered ALD on particles and ALD on nanotubes and nanorods. ALD on high aspect ratio structures was then considered including an examination of the times required for conformal growth on high aspect ratio structures. The ALD of nanolaminates and nanocomposites was discussed, including applications of the nanolaminates as thermal barrier coatings and Bragg X-ray mirrors. The overview then concluded with some additional topics such as area-selective ALD and atmospheric pressure ALD.

The future prospects for ALD are very promising. Various materials can be deposited using ALD techniques. The availability of many commercial ALD reactors continues to

make ALD accessible for many workers outside of the thin film growth community. ALD is firmly established on the *International Technology Roadmap for Semiconductors*. ALD should also play an integral role in new paradigms for electronic materials. The number of applications for ALD also continues to grow outside of the semiconductor arena. The future should see ALD continue to expand into new areas and find additional applications that benefit from its precise thickness control and conformality.

15. Acknowledgments

This overview of ALD is based in part on a one-day short course that SMG teaches for the AVS. The author thanks the AVS for the opportunity to develop and teach this course. In addition, the author acknowledges the students who have taken the course for their feedback and interests in various applications of ALD. SMG also thanks the National Science Foundation and the Air Force Office of Scientific Research for their research support on various aspects of ALD. This review would also not have been possible without the work of the many researchers in the ALD field. The author also thanks the past and former members of his research group for their contributions to ALD.

16. References

(1) *International Technology Roadmap for Semiconductors*, 2007 Edition, http://www.itrs.net/.
(2) Sneh, O.; Clark-Phelps, R. B.; Londergan, A. R.; Winkler, J.; Seidel, T. E. *Thin Solid Films* **2002**, *402*, 248.
(3) Paranjpe, A.; Gopinath, S.; Omstead, T.; Bubber, R. *J. Electrochem. Soc.* **2001**, *148*, G465.
(4) Chatham, H. *Surf. Coat. Technol.* **1996**, *78*, 1.
(5) George, S. M.; Ott, A. W.; Klaus, J. W. *J. Phys. Chem.* **1996**, *100*, 13121.
(6) Fabreguette, F. H.; Wind, R. A.; George, S. M. *Appl. Phys. Lett.* **2006**, *88*, 013116.
(7) Groner, M. D.; Elam, J. W.; Fabreguette, F. H.; George, S. M. *Thin Solid Films* **2002**, *413*, 186.
(8) Goodman, C. H. L.; Pessa, M. V. *J. Appl. Phys.* **1986**, *60*, R65.
(9) Niinisto, L. *Curr. Opin. Solid State Mater. Sci.* **1998**, *3*, 147.
(10) Niinisto, L.; Leskela, M. *Thin Solid Films* **1993**, *225*, 130.
(11) Suntola, T. *Thin Solid Films* **1992**, *216*, 84.
(12) Suntola, T. Atomic Layer Epitaxy. In *Handbook of Crystal Growth, Vol. 3, Part B: Growth Mechanisms and Dynamics*; Hurle, D. T. J., Ed.; Elsevier: Amsterdam, 1994; Chapter 14.
(13) Suntola, T.; Hyvarinen, J. *Annu. Rev. Mater. Sci.* **1985**, *15*, 177.
(14) Ott, A. W.; Klaus, J. W.; Johnson, J. M.; George, S. M. *Thin Solid Films* **1997**, *292*, 135.
(15) Nishizawa, J.; Abe, H.; Kurabayashi, T. *J. Electrochem. Soc.* **1985**, *132*, 1197.
(16) Suntola, T. Thirty Years of ALD. An Invited Talk at *AVS Topical Conference on Atomic Layer Deposition (ALD2004)*; University of Helsinki: Helsinki, Finland, August 16, 2004.
(17) Suntola, T.; Antson, J. Method for Producing Compound Thin Films. U.S. Patent #4,058,430, Issued Nov. 25, 1977.
(18) Ahonen, M.; Pessa, M.; Suntola, T. *Thin Solid Films* **1980**, *65*, 301.
(19) Leskela, M.; Ritala, M. *Thin Solid Films* **2002**, *409*, 138.
(20) Puurunen, R. L. *J. Appl. Phys.* **2005**, *97*, 121301.
(21) Ritala, M.; Leskela, M. Atomic Layer Deposition. *Handbook of Thin Film Materials*; San Diego, CA, 2001.
(22) Kim, H. *J. Vac. Sci. Technol. B* **2003**, *21*, 2231.
(23) Kim, H.; Lee, H. B. R.; Maeng, W. J. *Thin Solid Films* **2009**, *517*, 2563.
(24) Knez, M.; Niesch, K.; Niinisto, L. *Adv. Mater.* **2007**, *19*, 3425.
(25) Leskela, M.; Ritala, M. *Angew. Chem., Int. Ed.* **2003**, *42*, 5548.
(26) Niinisto, L.; Paivasaari, J.; Niinisto, J.; Putkonen, M.; Nieminen, M. *Phys. Status Solidi A* **2004**, *201*, 1443.
(27) Ritala, M.; Leskela, M. *Nanotechnology* **1999**, *10*, 19.
(28) Higashi, G. S.; Fleming, C. G. *Appl. Phys. Lett.* **1989**, *55*, 1963.
(29) Soto, C.; Tysoe, W. T. *J. Vac. Sci. Technol. A* **1991**, *9*, 2686.
(30) Goldstein, D. N.; McCormick, J. A.; George, S. M. *J. Phys. Chem. C* **2008**, *112*, 19530.
(31) Kim, J. B.; Kwon, D. R.; Chakrabarti, K.; Lee, C.; Oh, K. Y.; Lee, J. H. *J. Appl. Phys.* **2002**, *92*, 6739.
(32) Dillon, A. C.; Ott, A. W.; Way, J. D.; George, S. M. *Surf. Sci.* **1995**, *322*, 230.
(33) *HSC Chemistry*, 5.11 edition; Outokumpu Research Oy: Pori, Finland. Values are given at 0 °C.
(34) Widjaja, Y.; Musgrave, C. B. *Appl. Phys. Lett.* **2002**, *80*, 3304.
(35) Ferguson, J. D.; Weimer, A. W.; George, S. M. *Thin Solid Films* **2000**, *371*, 95.
(36) Ferguson, J. D.; Weimer, A. W.; George, S. M. *Chem. Mater.* **2004**, *16*, 5602.
(37) Juppo, M.; Rahtu, A.; Ritala, M.; Leskela, M. *Langmuir* **2000**, *16*, 4034.
(38) Rahtu, A.; Alaranta, T.; Ritala, M. *Langmuir* **2001**, *17*, 6506.
(39) Elam, J. W.; Groner, M. D.; George, S. M. *Rev. Sci. Instrum.* **2002**, *73*, 2981.
(40) Hakim, L. F.; Blackson, J.; George, S. M.; Weimer, A. W. *Chem. Vap. Deposition* **2005**, *11*, 420.
(41) McCormick, J. A.; Cloutier, B. L.; Weimer, A. W.; George, S. M. *J. Vac. Sci. Technol. A* **2007**, *25*, 67.
(42) Ritala, M.; Leskela, M.; Dekker, J. P.; Mutsaers, C.; Soininen, P. J.; Skarp, J. *Chem. Vap. Deposition* **1999**, *5*, 7.
(43) Groner, M. D.; Fabreguette, F. H.; Elam, J. W.; George, S. M. *Chem. Mater.* **2004**, *16*, 639.
(44) Huang, M. L.; Chang, Y. C.; Chang, C. H.; Lee, Y. J.; Chang, P.; Kwo, J.; Wu, T. B.; Hong, M. *Appl. Phys. Lett.* **2005**, *87*, 252104.
(45) Xuan, Y.; Lin, H. C.; Ye, P. D.; Wilk, G. D. *Appl. Phys. Lett.* **2006**, *88*, 263518.
(46) Ye, P. D.; Wilk, G. D.; Kwo, J.; Yang, B.; Gossmann, H. J. L.; Frei, M.; Chu, S. N. G.; Mannaerts, J. P.; Sergent, M.; Hong, M.; Ng, K. K.; Bude, J. *IEEE Electron Device Lett.* **2003**, *24*, 209.
(47) Ritala, M.; Leskela, M.; Nykanen, E.; Soininen, P.; Niinisto, L. *Thin Solid Films* **1993**, *225*, 288.
(48) Yamada, A.; Sang, B. S.; Konagai, M. *Appl. Surf. Sci.* **1997**, *112*, 216.
(49) Yousfi, E. B.; Fouache, J.; Lincot, D. *Appl. Surf. Sci.* **2000**, *153*, 223.
(50) Rossnagel, S. M.; Sherman, A.; Turner, F. *J. Vac. Sci. Technol. B* **2000**, *18*, 2016.
(51) Kim, H.; Cabral, C.; Lavoie, C.; Rossnagel, S. M. *J. Vac. Sci. Technol. B* **2002**, *20*, 1321.
(52) Grubbs, R. K.; George, S. M. *J. Vac. Sci. Technol. A* **2006**, *24*, 486.
(53) Coon, P. A.; Gupta, P.; Wise, M. L.; George, S. M. *J. Vac. Sci. Technol. A* **1992**, *10*, 324.
(54) Koehler, B. G.; Mak, C. H.; Arthur, D. A.; Coon, P. A.; George, S. M. *J. Chem. Phys.* **1988**, *89*, 1709.
(55) Gupta, P.; Coon, P. A.; Koehler, B. G.; George, S. M. *Surf. Sci.* **1991**, *249*, 92.
(56) Hasunuma, E.; Sugahara, S.; Hoshino, S.; Imai, S.; Ikeda, K.; Matsumura, M. *J. Vac. Sci. Technol. A* **1998**, *16*, 679.
(57) Imai, S.; Iizuka, T.; Sugiura, O.; Matsumura, M. *Thin Solid Films* **1993**, *225*, 168.
(58) Sugahara, S.; Kadoshima, M.; Kitamura, T.; Imai, S.; Matsumura, M. *Appl. Surf. Sci.* **1995**, *90*, 349.
(59) Sugahara, S.; Uchida, Y.; Kitamura, T.; Nagai, T.; Matsuyama, M.; Hattori, T.; Matsumura, M. *Jpn. J. Appl. Phys. Part 1* **1997**, *36*, 1609.
(60) Heil, S. B. S.; Kudlacek, P.; Langereis, E.; Engeln, R.; van de Sanden, M. C. M.; Kessels, W. M. M. *Appl. Phys. Lett.* **2006**, *89*, 131505.
(61) Langereis, E.; Creatore, M.; Heil, S. B. S.; Van de Sanden, M. C. M.; Kessels, W. M. M. *Appl. Phys. Lett.* **2006**, *89*, 081915.
(62) Lim, J. W.; Yun, S. J. *Electrochem. Solid-State Lett.* **2004**, *7*, F45.
(63) Hoex, B.; Heil, S. B. S.; Langereis, E.; van de Sanden, M. C. M.; Kessels, W. M. M. *Appl. Phys. Lett.* **2006**, *89*, 042112.
(64) Elam, J. W.; Schuisky, M.; Ferguson, J. D.; George, S. M. *Thin Solid Films* **2003**, *436*, 145.
(65) Kwon, O. K.; Kwon, S. H.; Park, H. S.; Kang, S. W. *J. Electrochem. Soc.* **2004**, *151*, C753.
(66) Rayner, G. B.; George, S. M. *J. Vac. Sci. Technol. A* **2009**, *27*, 716.
(67) Park, J. S.; Lee, M. J.; Lee, C. S.; Kang, S. W. *Electrochem. Solid-State Lett.* **2001**, *4*, C17.
(68) Park, J. S.; Park, H. S.; Kang, S. W. *J. Electrochem. Soc.* **2002**, *149*, C28.
(69) Van, T. T.; Chang, J. P. *Surf. Sci.* **2005**, *596*, 1.
(70) Knoops, H. C. M.; Mackus, A. J. M.; Donders, M. E.; van de Sanden, M. C. M.; Notten, P. H. L.; Kessels, W. M. M. *Electrochem. Solid-State Lett.* **2009**, *12*, G34.
(71) Kwon, O. K.; Kwon, S. H.; Park, H. S.; Kang, S. W. *Electrochem. Solid-State Lett.* **2004**, *7*, C46.
(72) Suntola, T.; Paakala, A. J.; Lindfors, S. G. *"Apparatus for Performing Growth of Compound Thin Films"*, U.S. Patent #4,389,973, Issued Jun. 28, 1983.
(73) Suntola, T. *Thin Solid Films* **1993**, *225*, 96.
(74) Sneh, O.; Wise, M. L.; Ott, A. W.; Okada, L. A.; George, S. M. *Surf. Sci.* **1995**, *334*, 135.

(75) Skarp, J. I.; Soininen, P. J.; Soininen, P. T. *Appl. Surf. Sci.* **1997**, *112*, 251.
(76) Dushman, S. *Scientific Foundations of Vacuum Technique*, 2nd ed.; Revised by Lafferty, J. M., Editor; John Wiley & Sons: New York, 1962.
(77) Roth, A. *Vacuum Technology*, 2nd, Revised Edition; North-Holland: Amsterdam, 1986.
(78) Sneh, O. ALD Apparatus and Method. U.S. Patent #6,911,092, Issued June 28, 2005.
(79) Sneh, O. Unpublished Information from Sundew Technologies, LLC, Broomfield, CO.
(80) Heil, S. B. S.; van Hemmen, J. L.; Hodson, C. J.; Singh, N.; Klootwijk, J. H.; Roozeboom, F.; de Sanden, M.; Kessels, W. M. M. *J. Vac. Sci. Technol. A* **2007**, *25*, 1357.
(81) Klaus, J. W.; Ferro, S. J.; George, S. M. *Thin Solid Films* **2000**, *360*, 145.
(82) Grubbs, R. K.; Steinmetz, N. J.; George, S. M. *J. Vac. Sci. Technol. B* **2004**, *22*, 1811.
(83) Fabreguette, F. H.; Sechrist, Z. A.; Elam, J. W.; George, S. M. *Thin Solid Films* **2005**, *488*, 103.
(84) Elam, J. W.; Nelson, C. E.; Grubbs, R. K.; George, S. M. *Surf. Sci.* **2001**, *479*, 121.
(85) Luoh, T.; Su, C. T.; Yang, T. H.; Chen, K. C.; Lu, C. Y. *Microelectron. Eng.* **2008**, *85*, 1739.
(86) Aaltonen, T.; Alen, P.; Ritala, M.; Leskela, M. *Chem. Vap. Deposition* **2003**, *9*, 45.
(87) Aaltonen, T.; Ritala, M.; Sajavaara, T.; Keinonen, J.; Leskela, M. *Chem. Mater.* **2003**, *15*, 1924.
(88) Aaltonen, T.; Rahtu, A.; Ritala, M.; Leskela, M. *Electrochem. Solid-State Lett.* **2003**, *6*, C130.
(89) Aaltonen, T.; Ritala, M.; Sammelselg, V.; Leskela, M. *J. Electrochem. Soc.* **2004**, *151*, G489.
(90) Aaltonen, T.; Ritala, M.; Leskela, M. *Electrochem. Solid-State Lett.* **2005**, *8*, C99.
(91) Kim, H.; Shimogaki, Y. *J. Electrochem. Soc.* **2007**, *154*, G13.
(92) Kim, H.; Kojima, Y.; Sato, H.; Yoshii, N.; Hosaka, S.; Shimogaki, Y. *Jpn. J. Appl. Phys. Part 2* **2006**, *45*, L233.
(93) Martensson, P.; Carlsson, J. O. *Chem. Vap. Deposition* **1997**, *3*, 45.
(94) Lampeonnerud, C.; Jansson, U.; Harsta, A.; Carlsson, J. O. *J. Cryst. Growth* **1992**, *121*, 223.
(95) Martensson, P.; Carlsson, J. O. *J. Electrochem. Soc.* **1998**, *145*, 2926.
(96) Huo, J. S.; Solanki, R.; McAndrew, J. *J. Mater. Res.* **2002**, *17*, 2394.
(97) Solanki, R.; Pathangey, B. *Electrochem. Solid-State Lett.* **2000**, *3*, 479.
(98) Elam, J. W.; Zinovev, A.; Han, C. Y.; Wang, H. H.; Welp, U.; Hryn, J. N.; Pellin, M. J. *Thin Solid Films* **2006**, *515*, 1664.
(99) Utriainen, M.; Kroger-Laukkanen, M.; Johansson, L. S.; Niinisto, L. *Appl. Surf. Sci.* **2000**, *157*, 151.
(100) Chae, J.; Park, H. S.; Kang, S. W. *Electrochem. Solid-State Lett.* **2002**, *5*, C64.
(101) Lim, B. S.; Rahtu, A.; Gordon, R. G. *Nat. Mater.* **2003**, *2*, 749.
(102) Argile, C.; Rhead, G. E. *Surf. Sci. Rep.* **1989**, *10*, 277.
(103) Besling, W. F. A.; Young, E.; Conard, T.; Zhao, C.; Carter, R.; Vandervorst, W.; Caymax, M.; De Gendt, S.; Heyns, M.; Maes, J.; Tuominen, M.; Haukka, S. *J. Non-Cryst. Solids* **2002**, *303*, 123.
(104) Copel, M.; Gribelyuk, M.; Gusev, E. *Appl. Phys. Lett.* **2000**, *76*, 436.
(105) Green, M. L.; Ho, M. Y.; Busch, B.; Wilk, G. D.; Sorsch, T.; Conard, T.; Brijs, B.; Vandervorst, W.; Raisanen, P. I.; Muller, D.; Bude, M.; Grazul, J. *J. Appl. Phys.* **2002**, *92*, 7168.
(106) Gusev, E. P.; Cabral, C.; Copel, M.; D'Emic, C.; Gribelyuk, M. *Microelectron. Eng.* **2003**, *69*, 145.
(107) Frank, M. M.; Chabal, Y. J.; Wilk, G. D. *Appl. Phys. Lett.* **2003**, *82*, 4758.
(108) Halls, M. D.; Raghavachari, K.; Frank, M. M.; Chabal, Y. J. *Phys. Rev. B* **2003**, *68*, 161302.
(109) Elam, J. W.; Nelson, C. E.; Grubbs, R. K.; George, S. M. *Thin Solid Films* **2001**, *386*, 41.
(110) Grubbs, R. K.; Nelson, C. E.; Steinmetz, N. J.; George, S. M. *Thin Solid Films* **2004**, *467*, 16.
(111) Sechrist, Z. A.; Fabreguette, F. H.; Heintz, O.; Phung, T. M.; Johnson, D. C.; George, S. M. *Chem. Mater.* **2005**, *17*, 3475.
(112) Nilsen, O.; Karlsen, O. B.; Kjekshus, A.; Fjellvag, H. *Thin Solid Films* **2007**, *515*, 4527.
(113) Nilsen, O.; Mohn, C. E.; Kjekshus, A.; Fjellvag, H. *J. Appl. Phys.* **2007**, *102*, 024906.
(114) Wind, R. A.; Fabreguette, F. H.; Sechrist, Z. A.; George, S. M. *J. Appl. Phys.* **2009**, *105*, 074309.
(115) Cavanagh, A. S.; Wilson, C. A.; Weimer, A. W.; George, S. M. *Nanotechnology* **2009**, *20*, 255602.
(116) Farmer, D. B.; Gordon, R. G. *Electrochem. Solid-State Lett.* **2005**, *8*, G89.
(117) Farmer, D. B.; Gordon, R. G. *Nano Lett.* **2006**, *6*, 699.
(118) Xuan, Y.; Wu, Y. Q.; Shen, T.; Qi, M.; Capano, M. A.; Cooper, J. A.; Ye, P. D. *Appl. Phys. Lett.* **2008**, *92*, 013101.
(119) Lee, B. K.; Park, S. Y.; Kim, H. C.; Cho, K.; Vogel, E. M.; Kim, M. J.; Wallace, R. M.; Kim, J. Y. *Appl. Phys. Lett.* **2008**, *92*, 203102.
(120) Wang, X. R.; Tabakman, S. M.; Dai, H. J. *J. Am. Chem. Soc.* **2008**, *130*, 8152.
(121) King, J. S.; Graugnard, E.; Roche, O. M.; Sharp, D. N.; Scrimgeour, J.; Denning, R. G.; Turberfield, A. J.; Summers, C. J. *Adv. Mater.* **2006**, *18*, 1561.
(122) Knez, M.; Kadri, A.; Wege, C.; Gosele, U.; Jeske, H.; Nielsch, K. *Nano Lett.* **2006**, *6*, 1172.
(123) Scharrer, M.; Wu, X.; Yamilov, A.; Cao, H.; Chang, R. P. H. *Appl. Phys. Lett.* **2005**, *86*.
(124) Klaus, J. W.; Ott, A. W.; Johnson, J. M.; George, S. M. *Appl. Phys. Lett.* **1997**, *70*, 1092.
(125) Kang, J. K.; Musgrave, C. B. *J. Appl. Phys.* **2002**, *91*, 3408.
(126) Klaus, J. W.; George, S. M. *Surf. Sci.* **2000**, *447*, 81.
(127) Klaus, J. W.; Sneh, O.; George, S. M. *Science* **1997**, *278*, 1934.
(128) Ferguson, J. D.; Smith, E. R.; Weimer, A. W.; George, S. M. *J. Electrochem. Soc.* **2004**, *151*, G528.
(129) Du, Y.; Du, X.; George, S. M. *J. Phys. Chem. C* **2007**, *111*, 219.
(130) Okamoto, Y. *J. Phys. Chem. B* **1999**, *103*, 11074.
(131) Du, Y.; Du, X.; George, S. M. *Thin Solid Films* **2005**, *491*, 43.
(132) Parks, G. A. *Chem. Rev.* **1965**, *65*, 177.
(133) Jung, S. H.; Kang, S. W. *Jpn. J. Appl. Phys. Part 1* **2001**, *40*, 3147.
(134) Wilson, C. A.; Grubbs, R. K.; George, S. M. *Chem. Mater.* **2005**, *17*, 5625.
(135) Carcia, P. F.; McLean, R. S.; Reilly, M. H.; Groner, M. D.; George, S. M. *Appl. Phys. Lett.* **2006**, *89*, 031915.
(136) Groner, M. D.; George, S. M.; McLean, R. S.; Carcia, P. F. *Appl. Phys. Lett.* **2006**, *88*, 051907.
(137) Carcia, P. F.; McLean, R. S.; Groner, M. D.; Dameron, A. A.; George, S. M. *J. Appl. Phys.* **2009**, *106*, 023533.
(138) Dameron, A. A.; Davidson, S. D.; Burton, B. B.; Carcia, P. F.; McLean, R. S.; George, S. M. *J. Phys. Chem. C* **2008**, *112*, 4573.
(139) Meyer, J.; Gorrn, P.; Bertram, F.; Hamwi, S.; Winkler, T.; Johannes, H. H.; Weimann, T.; Hinze, P.; Riedl, T.; Kowalsky, W. *Adv. Mater.* **2009**, *21*, 1845.
(140) Ghosh, A. P.; Gerenser, L. J.; Jarman, C. M.; Fornalik, J. E. *Appl. Phys. Lett.* **2005**, *86*, 223503.
(141) Park, S. H. K.; Oh, J.; Hwang, C. S.; Lee, J. I.; Yang, Y. S.; Chu, H. Y. *Electrochem. Solid-State Lett.* **2005**, *8*, H21.
(142) Potscavage, W. J.; Yoo, S.; Domercq, B.; Kippelen, B. *Appl. Phys. Lett.* **2007**, *90*, 253511.
(143) Ferrari, S.; Perissinotti, F.; Peron, E.; Fumagalli, L.; Natali, D.; Sampietro, M. *Org. Electron.* **2007**, *8*, 407.
(144) Fumagalli, L.; Natali, D.; Sampietro, M.; Peron, E.; Perissinotti, F.; Tallarida, G.; Ferrari, S. *Org. Electron.* **2008**, *9*, 198.
(145) Hyde, G. K.; Park, K. J.; Stewart, S. M.; Hinestroza, J. P.; Parsons, G. N. *Langmuir* **2007**, *23*, 9844.
(146) Peng, Q.; Sun, X. Y.; Spagnola, J. C.; Hyde, G. K.; Spontak, R. J.; Parsons, G. N. *Nano Lett.* **2007**, *7*, 719.
(147) Cooper, R.; Upadhyaya, H. P.; Minton, T. K.; Berman, M. R.; Du, X. H.; George, S. M. *Thin Solid Films* **2008**, *516*, 4036.
(148) Wang, X. D.; Graugnard, E.; King, J. S.; Zhong, L. W.; Summers, C. J. *Nano Lett.* **2004**, *4*, 2223.
(149) Shin, H. J.; Jeong, D. K.; Lee, J. G.; Sung, M. M.; Kim, J. Y. *Adv. Mater.* **2004**, *16*, 1197.
(150) Wilson, C. A.; McCormick, J. A.; Cavanagh, A. S.; Goldstein, D. N.; Weimer, A. W.; George, S. M. *Thin Solid Films* **2008**, *516*, 6175.
(151) Mayer, T. M.; Elam, J. W.; George, S. M.; Kotula, P. G.; Goeke, R. S. *Appl. Phys. Lett.* **2003**, *82*, 2883.
(152) Jessensky, O.; Muller, F.; Gosele, U. *Appl. Phys. Lett.* **1998**, *72*, 1173.
(153) Elam, J. W.; Routkevitch, D.; Mardilovich, P. P.; George, S. M. *Chem. Mater.* **2003**, *15*, 3507.
(154) Gordon, R. G.; Hausmann, D.; Kim, E.; Shepard, J. *Chem. Vap. Deposition* **2003**, *9*, 73.
(155) Hoivik, N. D.; Elam, J. W.; Linderman, R. J.; Bright, V. M.; George, S. M.; Lee, Y. C. *Sens. Actuators A* **2003**, *103*, 100.
(156) Herrmann, C. F.; Delrio, F. W.; Bright, V. M.; George, S. M. *J. Micromech. Microeng.* **2005**, *15*, 984.
(157) Scharf, T. W.; Prasad, S. V.; Dugger, M. T.; Kotula, P. G.; Goeke, R. S.; Grubbs, R. K. *Acta Mater.* **2006**, *54*, 4731.
(158) Bachmann, J.; Jing, J.; Knez, M.; Barth, S.; Shen, H.; Mathur, S.; Gosele, U.; Nielsch, K. *J. Am. Chem. Soc.* **2007**, *129*, 9554.
(159) Daub, M.; Knez, M.; Goesele, U.; Nielsch, K. *J. Appl. Phys.* **2007**, *101*, 09J111.
(160) King, J. S.; Neff, C. W.; Summers, C. J.; Park, W.; Blomquist, S.; Forsythe, E.; Morton, D. *Appl. Phys. Lett.* **2003**, *83*, 2566.
(161) Rugge, A.; Park, J. S.; Gordon, R. G.; Tolbert, S. H. *J. Phys. Chem. B* **2005**, *109*, 3764.
(162) Sechrist, Z. A.; Schwartz, B. T.; Lee, J. H.; McCormick, J. A.; Piestun, R.; Park, W.; George, S. M. *Chem. Mater.* **2006**, *18*, 3562.

(163) Biener, J.; Baumann, T. F.; Wang, Y. M.; Nelson, E. J.; Kucheyev, S. O.; Hamza, A. V.; Kemell, M.; Ritala, M.; Leskela, M. *Nanotechnology* **2007**, *18*, 055303.
(164) Elam, J. W.; Libera, J. A.; Pellin, M. J.; Zinovev, A. V.; Greene, J. P.; Nolen, J. A. *Appl. Phys. Lett.* **2006**, *89*, 053124.
(165) Pellin, M. J.; Stair, P. C.; Xiong, G.; Elam, J. W.; Birrell, J.; Curtiss, L.; George, S. M.; Han, C. Y.; Iton, L.; Kung, H.; Kung, M.; Wang, H. H. *Catal. Lett.* **2005**, *102*, 127.
(166) Hakim, L. F.; Vaughn, C. L.; Dunsheath, H. J.; Carney, C. S.; Liang, X.; Li, P.; Weimer, A. W. *Nanotechnology* **2007**, *18*, 345603.
(167) Weimer, M. A.; Hakim, L. F.; King, D. M.; Liang, X.; Weimer, A. W.; George, S. M.; Li, P.; Groner, M. D. *Appl. Phys. Lett.* **2008**, *92*, 164101.
(168) King, D. M.; Liang, X. H.; Carney, C. S.; Hakim, L. F.; Li, P.; Weimer, A. W. *Adv. Funct. Mater.* **2008**, *18*, 607.
(169) Hakim, L. F.; King, D. M.; Zhou, Y.; Gump, C. J.; George, S. M.; Weimer, A. W. *Adv. Funct. Mater.* **2007**, *17*, 3175.
(170) Ferguson, J. D.; Buechler, K. J.; Weimer, A. W.; George, S. M. *Powder Technol.* **2005**, *156*, 154.
(171) Wank, J. R.; George, S. M.; Weimer, A. W. *Powder Technol.* **2001**, *121*, 195.
(172) Wank, J. R.; George, S. M.; Weimer, A. W. *Powder Technol.* **2004**, *142*, 59.
(173) Wank, J. R.; George, S. M.; Weimer, A. W. *J. Am. Ceram. Soc.* **2004**, *87*, 762.
(174) McCormick, J. A.; Rice, K. P.; Paul, D. F.; Weimer, A. W.; George, S. M. *Chem. Vap. Deposition* **2007**, *13*, 491.
(175) Lee, J. S.; Min, B.; Cho, K.; Kim, S.; Park, J.; Lee, Y. T.; Kim, N. S.; Lee, M. S.; Park, S. O.; Moon, J. T. *J. Cryst. Growth* **2003**, *254*, 443.
(176) Min, B.; Lee, J. S.; Hwang, J. W.; Keem, K. H.; Kang, M. I.; Cho, K.; Sung, M. Y.; Kim, S.; Lee, M. S.; Park, S. O.; Moon, J. T. *J. Cryst. Growth* **2003**, *252*, 565.
(177) Herrmann, C. F.; Fabreguette, F. H.; Finch, D. S.; Geiss, R.; George, S. M. *Appl. Phys. Lett.* **2005**, *87*, 123110.
(178) Kukli, K.; Ihanus, J.; Ritala, M.; Leskela, M. *J. Electrochem. Soc.* **1997**, *144*, 300.
(179) Zaitsu, S.; Jitsuno, T.; Nakatsuka, M.; Yamanaka, T.; Motokoshi, S. *Appl. Phys. Lett.* **2002**, *80*, 2442.
(180) El-Sayed, M. A. *Acc. Chem. Res.* **2001**, *34*, 257.
(181) Costescu, R. M.; Cahill, D. G.; Fabreguette, F. H.; Sechrist, Z. A.; George, S. M. *Science* **2004**, *303*, 989.
(182) Swartz, E. T.; Pohl, R. O. *Rev. Mod. Phys.* **1989**, *61*, 605.
(183) Kumagai, H.; Toyoda, K.; Kobayashi, K.; Obara, M.; Iimura, Y. *Appl. Phys. Lett.* **1997**, *70*, 2338.
(184) Ishii, M.; Iwai, S.; Kawata, H.; Ueki, T.; Aoyagi, Y. *J. Cryst. Growth* **1997**, *180*, 15.
(185) Fabreguette, F. H.; George, S. M. *Thin Solid Films* **2007**, *515*, 7177.
(186) Elam, J. W.; George, S. M. *Chem. Mater.* **2003**, *15*, 1020.
(187) Elam, J. W.; Routkevitch, D.; George, S. M. *J. Electrochem. Soc.* **2003**, *150*, G339.
(188) Herrmann, C. F.; DelRio, F. W.; Miller, D. C.; George, S. M.; Bright, V. M.; Ebel, J. L.; Strawser, R. E.; Cortez, R.; Leedy, K. D. *Sens. Actuators A* **2007**, *135*, 262.
(189) Yoshimura, T.; Tatsuura, S.; Sotoyama, W. *Appl. Phys. Lett.* **1991**, *59*, 482.
(190) Du, Y.; George, S. M. *J. Phys. Chem. C.* **2007**, *111*, 8509.
(191) Shao, H. I.; Umemoto, S.; Kikutani, T.; Okui, N. *Polymer* **1997**, *38*, 459.
(192) Kubono, A.; Okui, N. *Prog. Polym. Sci.* **1994**, *19*, 389.
(193) George, S. M.; Yoon, B.; Dameron, A. A. *Acc. Chem. Res.* **2009**, *42*, 498.
(194) Adamcyzk, N. M.; Dameron, A. A.; George, S. M. *Langmuir* **2008**, *24*, 2081.
(195) Kim, A.; Filler, M. A.; Kim, S.; Bent, S. F. *J. Am. Chem. Soc.* **2005**, *127*, 6123.
(196) Putkonen, M.; Harjuoja, J.; Sajavaara, T.; Niinisto, L. *J. Mater. Chem.* **2006**, *17*, 664.
(197) Lee, J. S.; Lee, Y. J.; Tae, E. L.; Park, Y. S.; Yoon, K. B. *Science* **2003**, *301*, 818.
(198) Yoshimura, T.; Terasawa, N.; Kazama, H.; Naito, Y.; Suzuki, Y.; Asama, K. *Thin Solid Films* **2006**, *497*, 182.
(199) Yoshimura, T.; Ito, S.; Nakayama, T.; Matsumoto, K. *Appl. Phys. Lett.* **2007**, *91*, 033103.
(200) Yoshimura, T.; Tatsuura, S.; Sotoyama, W.; Matsuura, A.; Hayano, T. *Appl. Phys. Lett.* **1992**, *60*, 268.
(201) Dameron, A. A.; Saghete, D.; Burton, B. B.; Davidson, S. D.; Cavanagh, A. S.; Bertand, J. A.; George, S. M. *Chem. Mater.* **2008**, *20*, 3315.
(202) Peng, Q.; Gong, B.; VanGundy, R. M.; Parsons, G. N. *Chem. Mater.* **2009**, *21*, 820.
(203) Yoon, B.; O'Patchen, J. L.; Seghete, D.; Cavanagh, A. S.; George, S. M. *Chem. Vap. Deposition* **2009**, *15*, 112.
(204) Nilsen, O.; Fjellvag, H. Thin Films Prepared with Gas Phase Deposition Technique. Patent Cooperation Treaty (PCT), World Intellectual Property Organization, Publication Number WO 2006/071126 A1, Publication Date July 6, 2006.
(205) Lim, J. W.; Park, H. S.; Kang, S. W. *J. Electrochem. Soc.* **2001**, *148*, C403.
(206) Min, J. S.; Son, Y. W.; Kang, W. G.; Chun, S. S.; Kang, S. W. *Jpn. J. Appl. Phys. Part 1* **1998**, *37*, 4999.
(207) Ritala, M.; Leskela, M.; Rauhala, E.; Haussalo, P. *J. Electrochem. Soc.* **1995**, *142*, 2731.
(208) Chen, R.; Kim, H.; McIntyre, P. C.; Bent, S. F. *Chem. Mater.* **2005**, *17*, 536.
(209) Chen, R.; Kim, H.; McIntyre, P. C.; Porter, D. W.; Bent, S. F. *Appl. Phys. Lett.* **2005**, *86*, 191910.
(210) Park, K. J.; Doub, J. M.; Gougousi, T.; Parsons, G. N. *Appl. Phys. Lett.* **2005**, *86*, 051903.
(211) Chen, R.; Bent, S. F. *Adv. Mater.* **2006**, *18*, 1086.
(212) Park, K. S.; Seo, E. K.; Do, Y. R.; Kim, K.; Sung, M. M. *J. Am. Chem. Soc.* **2006**, *128*, 858.
(213) Sinha, A.; Hess, D. W.; Henderson, C. L. *J. Vac. Sci. Technol. B* **2006**, *24*, 2523.
(214) Sinha, A.; Hess, D. W.; Henderson, C. L. *J. Electrochem. Soc.* **2006**, *153*, G465.
(215) Liu, J. R.; Mao, Y. B.; Lan, E.; Banatao, D. R.; Forse, G. J.; Lu, J.; Blom, H. O.; Yeates, T. O.; Dunn, B.; Chang, J. P. *J. Am. Chem. Soc.* **2008**, *130*, 16908.
(216) Takahashi, N.; Yoshii, N.; Nonobe, S.; Nakamura, T.; Yoshioka, M. *J. Electron. Mater.* **2003**, *32*, 1107.
(217) Takahashi, N.; Nonobe, S.; Nakamura, T. *J. Solid State Chem.* **2004**, *177*, 3944.
(218) Levy, D. H.; Freeman, D.; Nelson, S. F.; Cowdery-Corvan, P. J.; Irving, L. M. *Appl. Phys. Lett.* **2008**, *92*, 192101.
(219) Sun, J.; Mourey, D. A.; Zhao, D. L.; Park, S. K.; Nelson, S. F.; Levy, D. H.; Freeman, D.; Cowdery-Corvan, P.; Tutt, L.; Jackson, T. N. *IEEE Electron Device Lett.* **2008**, *29*, 721.
(220) Huang, J. Y.; Wang, X. D.; Wang, Z. L. *Nano Lett.* **2006**, *6*, 2325.
(221) Gaillot, D. P.; Deparis, O.; Welch, V.; Wagner, B. K.; Vigneron, J. P.; Summers, C. J. *Phys. Rev. E* **2008**, *78*, 031922.
(222) Javey, A.; Kim, H.; Brink, M.; Wang, Q.; Ural, A.; Guo, J.; McIntyre, P.; McEuen, P.; Lundstrom, M.; Dai, H. J. *Nat. Mater.* **2002**, *1*, 241.
(223) Du, X.; George, S. M. *Sens. Actuators A* **2008**, *135*, 152.
(224) Martinson, A. B. F.; Elam, J. W.; Liu, J.; Pellin, M. J.; Marks, T. J.; Hupp, J. T. *Nano Lett.* **2008**, *8*, 2862.
(225) Nanu, M.; Schoonman, J.; Goossens, A. *Adv. Mater.* **2004**, *16*, 453.
(226) Finch, D. S.; Oreskovic, T.; Ramadurai, K.; Herrmann, C. F.; George, S. M.; Mahajan, R. L. *J. Biomed. Mater. Res. Part A* **2008**, *87A*, 100.

CR900056B